École polytechnique de Louvain

Determination of optimal power management strategies under operating uncertainty of a photovoltaic – battery – heat pump system with thermal storage

Author : **Maxime Vercoutere**
Supervisor : **Francesco Contino**
Readers : **Diederik Coppiters, Emmanuel De Jaeger**
Academic year 2020–2021
Master [120] in Electro-mechanical Engineering

Preface

This MSc thesis has been written to fulfill the graduation requirements of the Electromechanical Engineering program at UCLouvain.

I would like to thank Professor Francesco Contino, supervisor of this master thesis, for his precious advise, guidance and availability. Furthermore, I would like to thank Diederik Coppiters, mentor of this master thesis, for his precious help in carrying out this work. He was always ready to answer questions and give his time to explain specific details. Without him, the final results of this work would not be the same. Finally, I want to thank Professor Emmanuel De Jaeger, jury member, for taking the time to read this thesis and being present at the final presentation.

Enjoy the reading and I hope this work will reduce your uncertainties on operating your renewable energy system.

Maxime Vercoutere

Brussels, June 2021

Abstract

Balancing intermittent energy such as solar energy can be achieved by batteries, heat pumps and thermal storage tanks. This enables the coupling of the electricity and heating sectors. When the performances of such systems are evaluated, the parameters are often assumed as fixed and deterministic. Nevertheless, parameters such as grid electricity price, loads and investment costs are uncertain in reality. Moreover, power management strategies for combined operation are still an active research topic. To address these limitations, Robust Design Optimization (RDO) is performed on different power management strategies where uncertainties have been propagated. A photovoltaic - battery - heat pump - thermal storage tank system is studied for a household located in Belgium. First, the model undergoes the RDO using the NSGA-II algorithm and the Polynomial Chaos Expansion (PCE) method. Then, a comparison is made based on the performance of the different strategies. Finally, an analysis based on the stochastic performance of the different power management strategies is performed. The robust design optimization finds a trade-off between minimizing the Levelized Cost Of eXergy (LCOX) standard deviation and optimizing the levelized cost of exergy mean. This MSc thesis provides the optimized designs and the advantage of different power management strategies based on the financial flexibility of the household owner. The results demonstrate the possibility to reduce the impacts of the uncertainties on the system by having an improved strategy. Being able to sell its electricity surplus to the grid (i.e. grid selling strategy) allows obtaining a lower LCOX mean and LCOX standard deviation than the reference case (up to 20% and 13% respectively). Operating the system differently during the peak and off-peak hours (i.e. peak shaving strategy) or by doing a day ahead forecast (i.e. forecast strategy) also gives improved results regarding the reference case (up to 1.2% and

4.5% respectively for the LCOX standard deviation). However, a method based on buying electricity from the grid at low prices (i.e. grid buying strategy) shows weaker results regarding the LCOX standard deviation and the LCOX mean (up to 14% and 9% respectively). Subsequently, the uncertainty quantification shows that the uncertainties on the future grid electricity price and electricity load are dominant for the system (mean effect of 46% and 28% respectively on the robust designs). Finally, if the system owner predefines an upper limit of 550€/MWh, selling its electricity surplus achieves a higher probability than the reference case (i.e. 35%) of being lower than this limit. Having a different operation during peak and off-peak hours or doing a day ahead forecast improves the results regarding the reference case (i.e. both of 8%).

Keywords: Robust design optimization, NSGA-II, polynomial chaos expansion, power management strategies, levelized cost of exergy, Sobol' indices

Nomenclature

Acronym	Description
AC	Alternating Current
ASHP	Air-Source Heat Pump
CAPEX	CApital EXpenditure
CDF	Cumulative Density Function
COP	Coefficient Of Performance
DC	Direct Current
GA	Genetic Algorithm
LCOX	Levelized Cost Of eXergy
MPPT	Maximum Power Point Tracking
NSGA-II	Fast Non dominated Sorting Genetic Algorithm II
OPEX	OPerating EXpenditure
PCE	Polynomial Chaos Expansion
PV	PhotoVoltaic
RDO	Robust Design Optimization
SOC	State Of Charge
UQ	Uncertainty Quantification

Roman symbol	**Description**
C	Capacity
$C_{e,a}$	Grid electricity cost
$C_{r,a}$	Replacement cost
$C_{s,a}$	Grid electricity profit
D	Total variance
E	Electric energy
F	Carnot coefficient
I	Current
I_0	Reverse saturation current
N	Number of cells
n	System capacities
P	Power
Q	Heat
S	Sobol' index
R	Resistance
T	Temperature
U	Voltage
W	Work
X	Exergy

Subscript	Description
a	Annualized
amb	Ambient
bat	Battery
ch	Charge
d	Stochastic dimension
dch	Discharge
exc	Excess
L	Photogenerated
max	Maximum
min	Minimum
nom	Nominal
oc	Open-circuit
rem	Remaining
s	Series
sh	Shunt
wtank	Water tank

Greek symbol	Description
η	Efficiency
μ	Mean
σ	Standard deviation
ψ	Orthogonal polynomial

Contents

List of Figures

Chapter 1

Introduction

The deployment of intermittent renewable energy sources, such as solar energy, accelerates worldwide. Distributed solar PhotoVoltaic (PV) capacity is expected to nearly triple its capacity growth between 2019 and 2024 (406 GW) as opposed to 2012-2018 (142GW) [1]. Energy storage systems such as batteries and heat pumps match this intermittent energy source with the energy demand. Battery energy storage provides a flexible and adequate technology to improve the PV self-consumption [2]. In addition, heat pump and thermal storage, which cover the heat demand, further improve the PV self-consumption and entail the coupling of electricity and heating sector [3, 4].

While the advantages of each system are characterized in the literature [5, 6], power management strategies are still an active research topic. During these researches, techno-economic parameters are assumed fully known. However, parameters such as solar irradiance, ambient temperature, grid electricity price and investment costs are uncertain in reality. Consequently, these uncertainties should be considered in design and feasibility studies to shape the stochastic space under which decisions should be taken [7]. A common method that propagates parameter uncertainties through a system model and quantifies the statistical moment of the objective is the Monte Carlo Simulation. This method is robust and easy to implement, but it requires a significant number of model evaluations ($10^4 - 10^5$). When the model evaluation time is in the order of the minutes, this method becomes computationally infeasible. To reduce the computational time, a surrogate model is constructed on this model based on a limited number of system model evaluations [8]. A commonly used surrogate model for uncertainty quantification is the Polynomial Chaos Expansion (PCE) method [9]. PCE provides significant advantages, such as the analytic quantification of the statistical moments and the Sobol' indices out of the PCE coefficients. When the mean and standard deviation of a system objective can be quantified, these statistical moments can be used as optimization objectives (i.e. Robust Design Optimization (RDO)). A Pareto set of optimized designs can be found through a multi-objective optimization algorithm that makes a trade-off between minimizing the objective mean and minimizing the objective standard deviation. The design leading to the minimum standard deviation on the objective, the robust design, is the least sensitive to the parameter uncertainties. The robust design of the system can be further improved depending on the power management strategies used [10]. Depending on how the system handles the electricity surplus produced by the PV array, the system is subjected to different uncertainties.

This master thesis aims to determine and evaluate different power management strategies for energy systems under uncertainty. The main objective is to assess the impact of the uncertainties on the various power management strategies and to draw conclusions on which strategies to use to minimize the uncertainties.

The second chapter of this thesis relates to the system model, climate and demand data and the RDO. The descriptions of the different power management strategies are presented in Chapter 3. The optimized designs and results of the uncertainty propagation are shown in Chapter 4 and completed by the main conclusions of this work in Chapter 5. Finally, in Chapter 6, future possibilities of work are suggested.

Chapter 2

Method

The purpose of this chapter is to describe the system and optimization process. It will first explain the different models used for the system components. Subsequently, the hourly climate and demand data will be clarified. Finally, the robust design optimization framework will be explained. This includes the optimization algorithm and the uncertainty quantification method.

2.1 System model

The studied model is a household located in Belgium connected to the power grid and supported by a PhotoVoltaic (PV) array to cover the electricity demand. An Air-Source Heat Pump (ASHP) connected to a thermal storage tank with an electric heater is used to meet the heat demand (Figure 2.1). The grid is considered permanently available and able to cover the required power at any time of the year. A typical power management strategy is implemented between the different system components [10]. When there is a PV electricity excess, the electricity is first stored in the battery stack and then used to power the heat pump. On the opposite, when the PV array does not meet the electricity demand, the battery stack is first discharged and then the power grid is used if needed. If the thermal stored energy is insufficient to cover the heat demand, the ASHP complies with the remaining heat load. Suppose the PV excess can not run the ASHP, electricity from the grid supplies the ASHP. An electric heater supplied by the grid cover the remaining heat load at a fixed 99% efficiency [11] when the ASHP and thermal storage tank do not comply with the heat demand. The modeling has been done in Python™. The script has been provided by the assistant and adapted according to the different power management strategies.

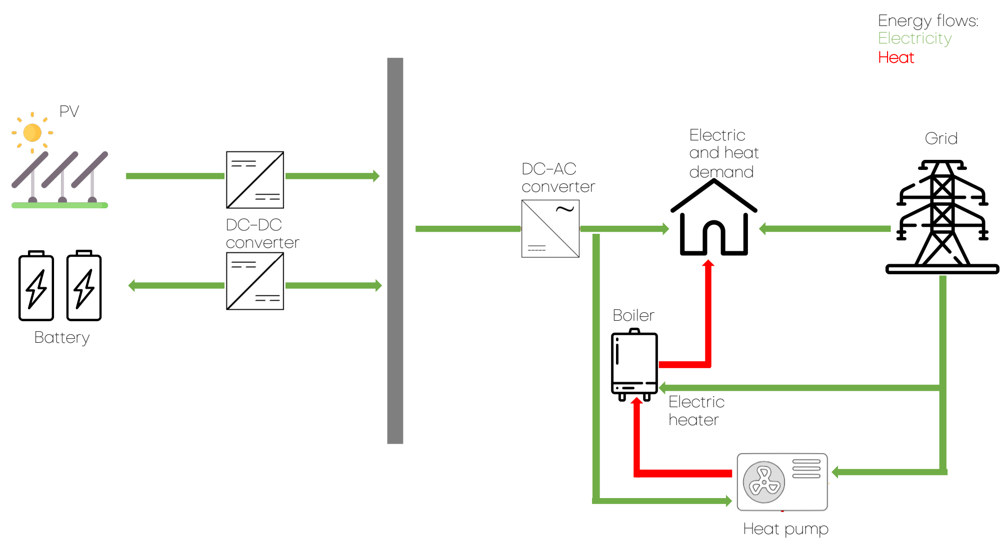

Figure 2.1: Schematic of the model located in Belgium, including the household connected to the grid and supported by a PhotoVoltaic (PV) array. The PV electricity excess charges the battery and powers the heat pump used to meet the electricity and heat demand. The grid is used when additional electricity is needed to cover the electricity demand or supply the heat pump and electric heater.

2.1.1 PhotoVoltaic array (PV)

The experimentally validated model of the PVLib Python library has been used [12] to calculate the amount of power produced by the PV array. It uses the following single-diode equation:

$$I_{\mathrm{PV}} = I_{\mathrm{L}} - I_0(\exp(\frac{U + IR_{\mathrm{s}}}{n_{\mathrm{diode}} N_{\mathrm{s}} U_{\mathrm{th}}}) - 1) - \frac{U + IR_{\mathrm{s}}}{R_{\mathrm{sh}}} \tag{2.1}$$

Thanks to the PVlib Python library, it is possible to calculate the five parameter values in

Equation 2.1 at effective irradiance and cell temperature using the De Soto et al. model described in [13]. The resulting current-voltage characteristic provides the power output. The PV array is connected to a DC-DC converter with Maximum Power Point Tracking (MPPT), where the maximum power point is assumed as the produced electric power by the PV array at each hour.

2.1.2 Battery stack

The lead-acid battery technology simulates electricity storage. The choice has been made of using a lead-acid battery instead of a lithium-ion battery because the current information and experiences available on the lithium-ion battery are quite limited [14]. Moreover, the uncertainty on the cost is still large [15]. This is an important aspect. Accurate information on the uncertainties is needed to perform the best RDO possible. The experimentally validated model of Blaifi et al. is used [16] to characterize the battery stack. The voltage-current relation for the lead-acid battery is defined as:

$$U_{\text{bat}} = U_{\text{bat,oc}} + I_{\text{bat}} R_{\text{bat}} \tag{2.2}$$

Where in Equation 2.2, $U_{\text{bat,oc}}$ is defined as the open circuit voltage, I_{bat} as the current which is provided or extracted during the charge and discharge and finally R_{bat}, the resistance component which determines the voltage evolution after charging and discharging the battery.

Another important parameter is the State of Charge (SOC). The SOC represents the fraction of the total capacity stored in the battery:

$$\text{SOC}(t) = \text{SOC}_0 + \frac{1}{C(t)} \int_0^t \eta_{bat}(t) I(t) dt \tag{2.3}$$

A minimum SOC of 20% is assumed [17, 18]. The battery lifetime is significantly affected by the SOC and is calculated through the Rainflow cycles counting method [19]. To avoid overcharging and overdischarging, which may cause excessive reduction of lifetime, the maximum charge and discharge current are limited to $C_{\text{nom}}/10$ and $C_{\text{nom}}/3.3$, respectively [20]. A daily discharging rate and a fixed energy efficiency of 80% have been assumed [21, 22].

2.1.3 Air-Source Heat Pump (ASHP)

The heat pump is an air-to-water, on/off-controlled heat pump, which uses ambient air as a heat source. It was first modeled as a refrigeration cycle using the CoolProp Python library [23]. For the sake of speed, the Coefficient Of Performance (COP) was approximated. Instead of calculating the enthalpy of the working fluid at each state of the refrigeration cycle, a second-order approximation has been made between the COP and the ambient temperature. This approach has been conducted by G. Angenendt et al. [24]. The framework was running 10 seconds faster, which is a considerable time saver during the RDO.

2.1.4 Thermal storage tank

The thermal storage tank is a stratified system for which the lower and upper temperature determine the thermal storage capacity. Considering the domestic hot water temperature of 40°C, the lower temperature is set at 45°C. The upper temperature is limited to 55°C.

2.1.5 Power converters

The PV array and the battery stack are connected to a DC-DC busbar through DC-DC converters. The DC busbar is connected through a DC-AC converter to provide electricity to the load or power grid. The conversion efficiency of the DC-DC converter is fixed at 95% [25, 26]. For the DC-AC inverter, the efficiency is set at 90% [27].

2.2 Climate and demand data

This model is based on hourly climate, electricity and heat demand characteristics. In this work, a household in Belgium is evaluated. To do so, the Typical Meteorological Year data and demand data from the National Renewable Energy Laboratory have been used [28, 29]. These data only exist for locations in the United States of America. With the method presented by Montero Carrero et al., it is possible to adapt climate and demand profiles for Belgium with typical scaling factors [30]. The climate and demand data used in this work are illustrated in Figure 2.2.

2.3 Robust Design Optimization (RDO)

2.3.1 Quantity of interest and design variables

The quantity of interest is the Levelized Cost Of eXergy (LCOX). This quantity can take into account the usefulness of available heat and electricity energy [31]. The LCOX reflects the system cost per unit of exergy covered [17]:

$$\mathrm{LCOX} = \frac{\mathrm{CAPEX_a} + \mathrm{OPEX_a} + \mathrm{C_{r,a}} + \mathrm{C_{e,a}} - \mathrm{C_{s,a}}}{\mathrm{X_{demand}}} \tag{2.4}$$

To determine the annual system cost, the annualized investment cost ($\mathrm{CAPEX_a}$), operational cost ($\mathrm{OPEX_a}$), replacement cost ($\mathrm{C_{r,a}}$), grid electricity cost ($\mathrm{C_{e,a}}$) and grid selling electricity profit (-$\mathrm{C_{s,a}}$) are added together.

The quantity of each parameter can be found in Zakeri et al. [17]. The annual exergy demand ($\mathrm{X_{demand}}$) can be calculated as the sum of the annual exergy required for electricity and heating demand [32]:

$$\sum_{i=1}^{8760} \sum_{\mathrm{type}} X_{\mathrm{type}}, \qquad \mathrm{type} \in \{\mathrm{elec, heat}\} \tag{2.5}$$

The electricity has the highest energy quality, the exergy is equal to the electricity load, $\mathrm{X_{elec}}$=$\mathrm{P_{elec}}$. To recover the exergy of the heat demand, the Carnot coefficient (F) is used to scale the demand [32]:

$$\mathrm{X_{heat}} = \mathrm{F_{heat}} \mathrm{P_{heat}}, \tag{2.6}$$

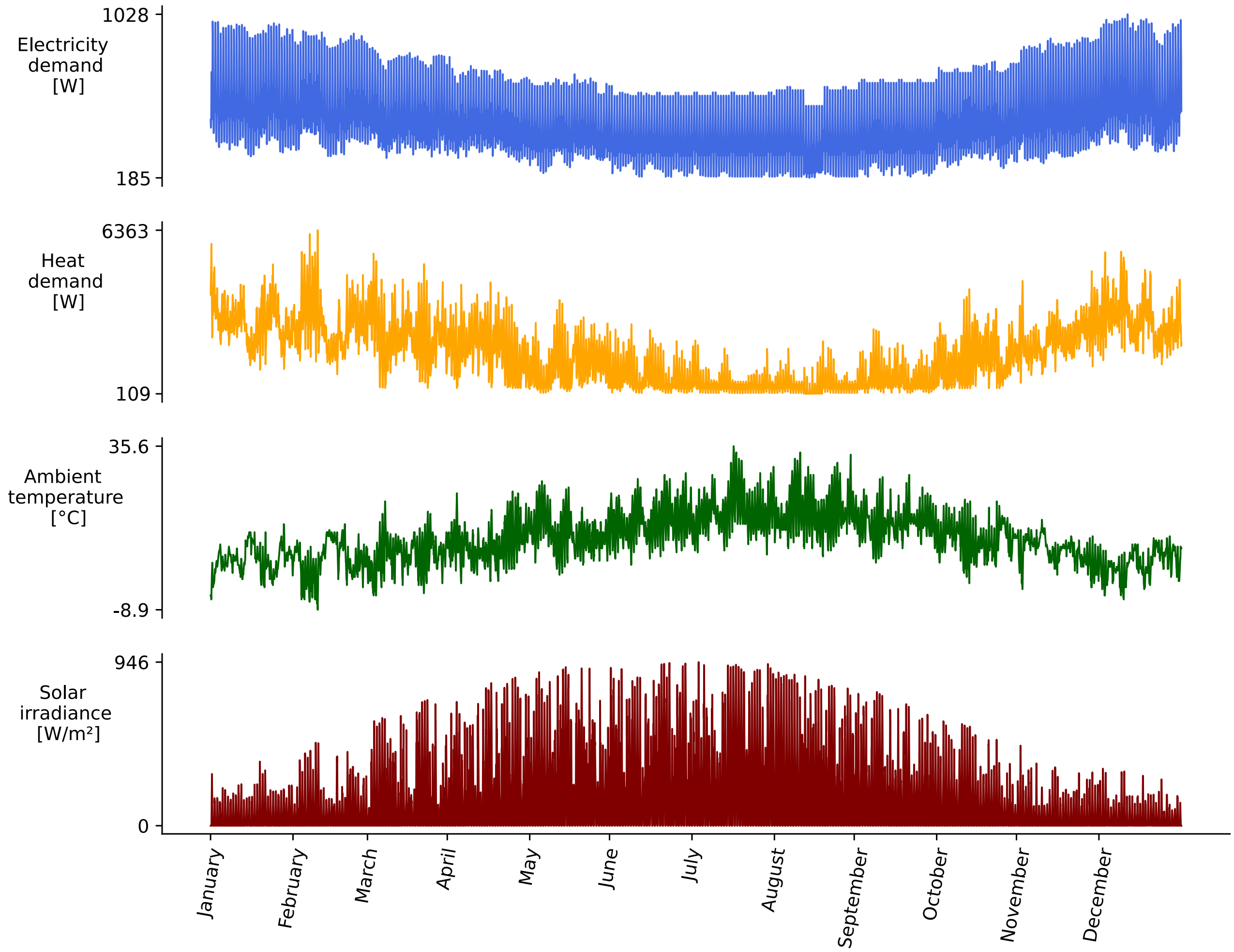

Figure 2.2: Typical climate (solar irradiance and ambient temperature) and loads data for a household in Belgium. The climate and load data are inversely proportional, which results in a PV power excess during the summer and a lack of electricity during the winter.

$$F_{heat} = 1 - \frac{T_{amb}}{T_{req}} \tag{2.7}$$

Where P_{heat} corresponds to the heat load, T_{amb} represents the ambient temperature and T_{req} stands for the required temperature for the heat demand.

In this work, the capacity of the PV array (n_{PV}), battery stack (n_{bat}), heat pump (n_{ASHP}) and thermal storage tank (n_{wtank}) are the design variables. By considering the capacities as independent design variables, the optimization algorithm is able to exclude any technology from the model.

2.3.2 Optimization algorithm

In this work, an optimization algorithm needs to be selected which can handle multiple objectives. There are two main types of mathematical methods that can handle this problem, derivative-based and derivative-free (or heuristic) algorithms. The first type finds the optimum of differentiable functions such as linear programming and Lagrangian function relaxation [33]. Derivative-free methods use a set of population samples that evolves after each iteration towards the optimal solution. Because of this iteration process, these methods are often called evolutionary optimization algorithms. An example of this method is the Genetic Algorithm (GA). This algorithm is based on biological evolution in order to solve the problem. The algorithm first creates a random population of samples. Each sample is evaluated within the objective functions. Only the samples having the best fitness survive. They are the parents. The new population of samples is produced from the previous samples by either making random changes to a single sample (mutation) or by combining the vector entries of a pair of samples (crossover) [34].
There is often a trade-off between each objective. Each objective has an optimal solution that can not be improved without degrading another objective. This solution is called a Pareto optimal. All the Pareto optimals combined create a Pareto front.

The implemented algorithm for the optimization of the model is based on GA called NSGA-II (Fast Non dominated Sorting Genetic Algorithm II). It has the advantage that it is an efficient and well-used algorithm for the formation of non-dominated Pareto fronts [35]. The algorithm first creates a set of design samples based on Latin Hypercube Sampling [36]. Subsequently, the second population is made by crossover and mutation, as explained previously. The script is based on the existing Python library, UQPy, used for optimization and Uncertainty Quantification (UQ) [37]. A computational budget of 180,000 iterations has been given to the optimizer for each strategy to reach the optimal Pareto front [38]. The optimization algorithm is characterized with a mutation and crossover probability of 0.1 and 0.9, respectively.

2.3.3 Uncertainty characterization

The same reasoning is applicable for electricity and heat demand, where various predictions represent the unknown future evolution [39, 40]. The CAPEX of the different components can be considered uncertain due to the significant time frame between the design stage and investment stages and the evolving market conditions. The uncertainties have been characterized by a uniform distribution based on literature. A uniform distribution is the best guess of the actual unknown distribution of these uncertainties by giving them an equal probability. The uncertainties used in this work are illustrated in Table 2.1. In order to see the impact of these uncertainties on the outcome, an UQ method is used.

2.3.4 Uncertainty Quantification (UQ)

A mathematical way to describe the problem for a model $\mathcal{M}$ is [9]:

$$Y = \mathcal{M}(\boldsymbol{x}) \tag{2.8}$$

Where Y is the quantity of interest and $\boldsymbol{x}$ is the vector of independent random parameters, $\boldsymbol{x} = x_1, x_2, ..., x_d$, where d is the dimension of the stochastic space. The chosen UQ method to represent the response of the model is the Polynomial Chaos Expansion (PCE). The PCE representation of the model consists of a series of multivariate orthonormal polynomials ψ_{i} in the basis functions with corresponding coefficients u_{i} and is expressed as follows:

Parameter	Max	Min	Unit	Ref.
Electricity demand	0.8	1.2	none	[40, 41]
Heat demand	0.8	1.2	none	[39, 41]
Electricity cost	57	90	€/MWh	[42, 43]
CAPEX PV	350	600	€/$\mathrm{kW_p}$	[44]
CAPEX battery	102	354	€/kWh	[18]
CAPEX ASHP	600	1100	€/$\mathrm{kW_{th}}$	[45]
CAPEX thermal storage tank	2.8	5.4	€/l	[46, 47]
Discount rate	5	7	%	[48, 49, 50]

Table 2.1: Parameters affected by uncertainty. They are characterized by their unknown future evolution. These parameters will be propagated in the robust design optimization.

$$\hat{\mathcal{M}}(\boldsymbol{x}) = \sum_{i=0}^{P} u_i \psi_i(\boldsymbol{x}) \tag{2.9}$$

When the PCE is infinite, it forms an exact representation of the model. However, calculating the coefficients of an infinite series is impossible. A truncated scheme is implemented which include all polynomials op to a certain degree p [51]. As a result, the total number of terms retained in the PCE is equal to:

$$P + 1 = \frac{(d+p)!}{d!p!} \tag{2.10}$$

To compute the polynomial coefficients u_i, the preferred approach is the regression method [52]. It is generally recommended to use over-sampling to improve the accuracy of the polynomial coefficients. The regression coefficients u_i are then calculated using a least-squares method where the sum of the squares of the error is minimized [53]. It has been found in the literature that an oversampling ratio of 2 gives a better approximation of the polynomial coefficients [54]. This translates into a number of $2(P+1)$ training samples that are needed. From this regression, it will be possible to find the coefficients. When all coefficients are quantified, the mean μ and standard deviation σ of the objective follow analytically:

$$\mu = u_0 \tag{2.11}$$

$$\sigma^2 = \sum_{i=1}^{P} u_i^2 \tag{2.12}$$

2.3.5 Sobol' indices retrieved from the Polynomial Chaos Expansion (PCE)

Knowing the contribution of each stochastic parameter on the variation of the output can be a good indicator of the impact of each stochastic parameter on the outcome. Sobol' indices have proven to be the most efficient sensitivity measure for general computational models [9]. They can be directly obtained by the PCE method by post-processing of the coefficients. The Sobol' indices are defined as the ratio of the partial variances $D_{\boldsymbol{u}}$ to the total variance D, where $\boldsymbol{u}$ is a subset of variables of the d uncertain parameters ($\boldsymbol{u} \in [1, 2, ..., d]$) [9]. The first order Sobol' index, S_i^{PCE}, corresponds to a single input variable (i.e. $\boldsymbol{u} = \{i\}$). It is equal to the ratio of the partial variance of the corresponding input parameter i to the total variance D:

$$S_i^{\text{PCE}} = \frac{D_i}{D} = \frac{\text{Var}(\mathcal{M}_i[x_i])}{\text{Var}[\boldsymbol{y}]} \tag{2.13}$$

The second order Sobol' index (i.e. $\boldsymbol{u} = \{i, j\}$) is equal to:

$$S_{ij}^{PCE} = \frac{D_{ij}}{D} = \frac{\text{Var}[\mathcal{M}_{ij}(x_i, x_j)]}{\text{Var}[\boldsymbol{y}]} \tag{2.14}$$

First-order indices, S_i^{PCE}, describe the influence of each variable considered separately as the main effect. Second-order indices, S_{ij}^{PCE}, describe the effects of the interaction between the variables x_i and x_j. The total Sobol' index, $S_i^{T,PCE}$, quantifies the total impact of a given parameter, x_i, including all interactions. It may be computed by the sum of the Sobol' indices of any order that contain x_i [55]:

$$S_i^{T,PCE} = \sum_{i \in \boldsymbol{u}} S_{\boldsymbol{u}}^{PCE} \tag{2.15}$$

Chapter 3

Description of the strategies

This chapter describes the different power management strategies, which will be subjected to the robust design optimization. Each strategy includes the models, loads and climate data introduced in the previous chapter. This section will present one reference strategy and six different power management strategies. Out of the six strategies, the two first strategies take advantage of the variable wholesale price. The two middle ones focus on the use of the heat pump and the two final strategies have an overall different operation of the system.

3.1 Reference strategy

When the power generated by the PV array (P_{PV}) is higher than the electricity demand ($P_{elec,load}$), the battery is first charged if the state of charge (SOC) is below the maximal state of charge (SOC_{max}). The battery is charged with the power excess produced (P_{exc}) and charged with a current (I_{ch}) below one-tenth of the nominal capacity (C_{nom}) of the battery. This is done to avoid overcharging, which may cause excessive reduction of lifetime [20]. Then, the power surplus is decreased by the amount of power charged to the battery (P_{bat}). Afterwards, the thermal storage tank is discharged to recover the heat load. If the temperature of the water tank (T_{wtank}) falls below the minimum temperature ($T_{min,wtank}$), the ASHP operates with the power excess. If not, the new temperature of the tank is calculated. The ASHP is always running at its maximum power (W_{max}). If the power surplus is below W_{max}, then the grid is used to buy electricity to reach the maximal power of the heat pump. Subsequently, the ASHP will produce an amount of thermal energy (Q), which is transferred to the thermal storage tank. If the tank's temperature is still below the minimum temperature, an electric heater powered directly by the grid is used. If not, the new temperature is calculated.

When the electricity demand is higher than the power generated by the PV, a remaining load (P_{rem}) has to be covered. If the SOC of the battery is greater than the minimum state of charge (SOC_{min}), the battery is discharged with a current (I_{dch}) below one-third of the nominal capacity of the battery. This is done to avoid overdischarging, which may cause excessive reduction of lifetime [20]. Suppose the power retrieved by the battery (P_{bat}) is not equal to the remaining load, the grid is used to buy the difference. For the heat load, the same steps are followed as explained earlier, except that the ASHP is directly run with energy from the grid because there is no power excess.

The decision tree of this strategy is illustrated in Figure 3.1.

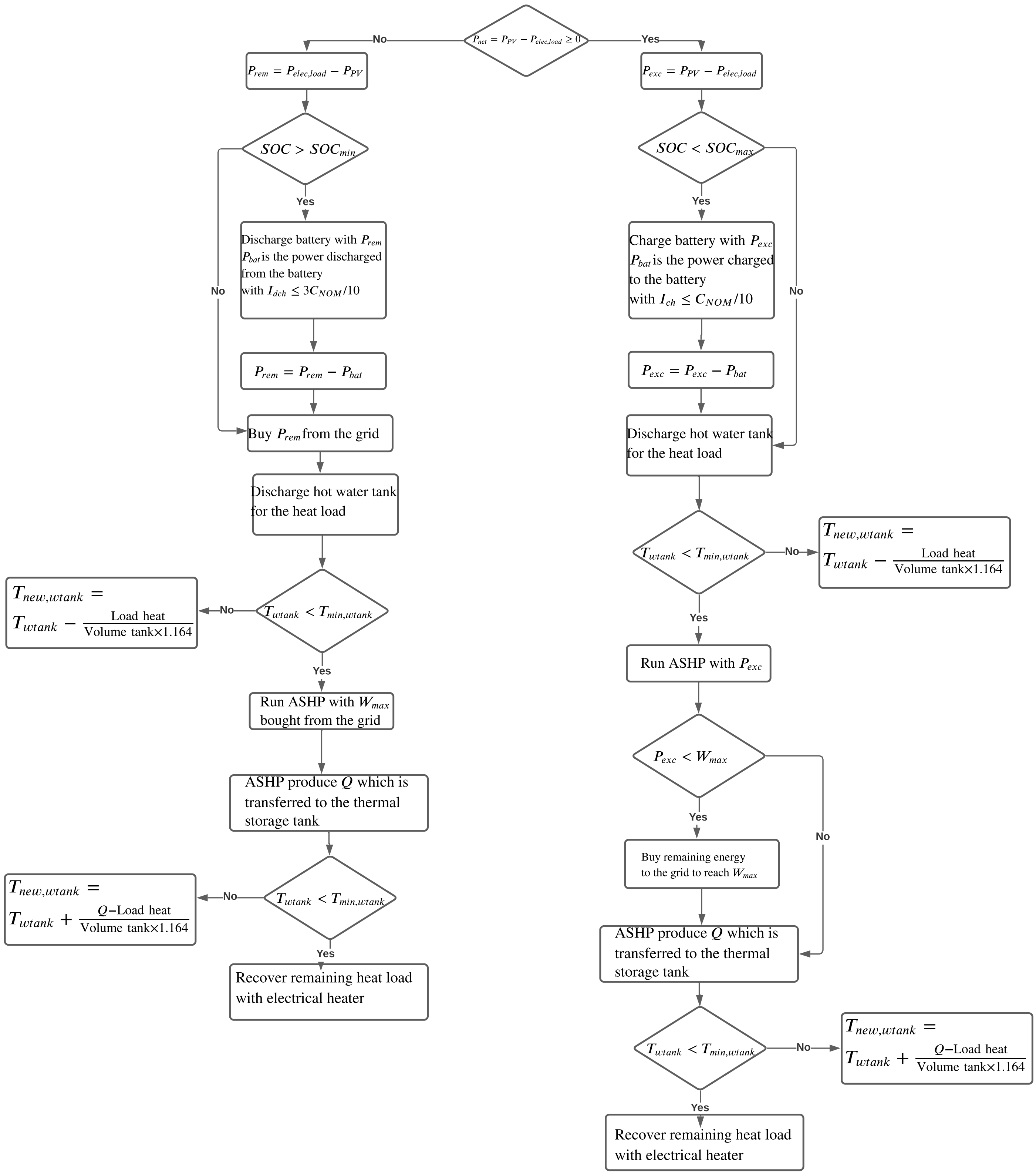

Figure 3.1: Decision tree for the reference strategy. When there is PV electricity excess, the electricity is first stored in the battery stack and then used to power the heat pump. When the PV array does not meet the electricity demand, the battery stack is first discharged and then power from the grid is used if needed.

3.2 Grid buying strategy

This first strategy focuses on buying energy from the grid when the wholesale price is low to recover the remaining load. This strategy aims to understand if it is more efficient in a techno-economic way to buy electricity from the grid instead of discharging the battery. To do so, a new design variable, low_price, is implemented in the framework. The strategy operates as follows: when the power generated by the PV array is higher than the demand, the system follows the steps explained in the reference case (see Section 3.1). When the electricity load is higher than the power generated by the PV array, if the hourly price of electricity (electricity_price) is cheaper than low_price, the grid is used to recover the electricity demand. The battery is not discharged. If not, the regular operation is followed as described in Section 3.1.

The decision tree of this strategy is illustrated in Figure 3.2.

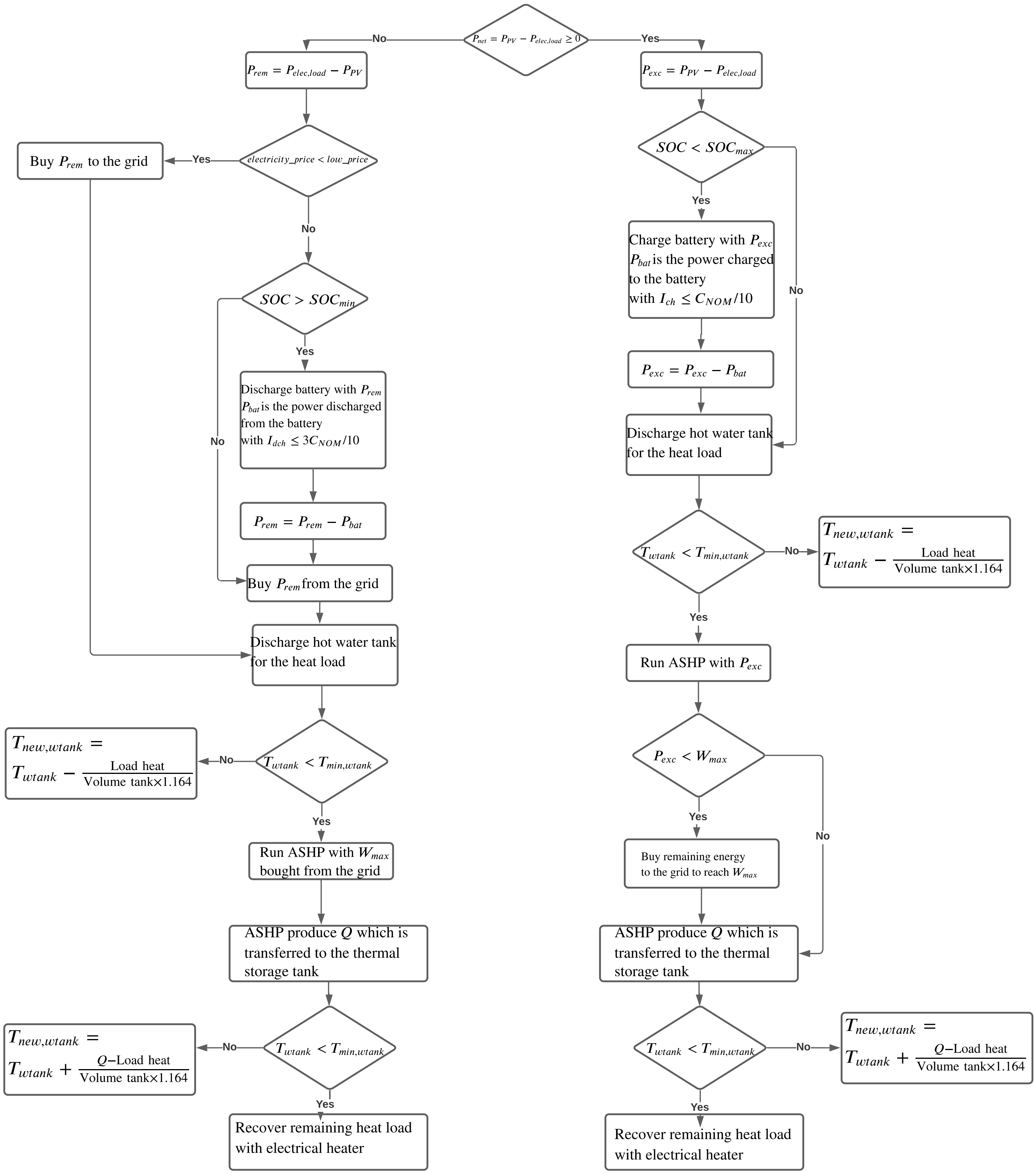

Figure 3.2: Decision tree for the grid buying strategy, a new design variable is included, low_price. When the electricity price is lower than this threshold variable, the grid is directly used to recover the load instead of discharging the battery.

3.3 Grid selling strategy

This second strategy focuses on selling energy from the grid when the wholesale price is high. This strategy aims to understand if it is more efficient in a techno-economic way to sell electricity to the grid. To do so, a new design variable, $high\_price$, is implemented in the framework. The strategy operates as follows: when the power generated by the PV array is higher than the electricity demand, if the hourly price of electricity is greater than $high\_price$, the energy excess is directly sold to the grid instead of charging the battery. If not, the regular operation is followed as described in Section 3.1 and the system can sell its energy surplus.

The decision tree of this strategy is illustrated in Figure 3.3.

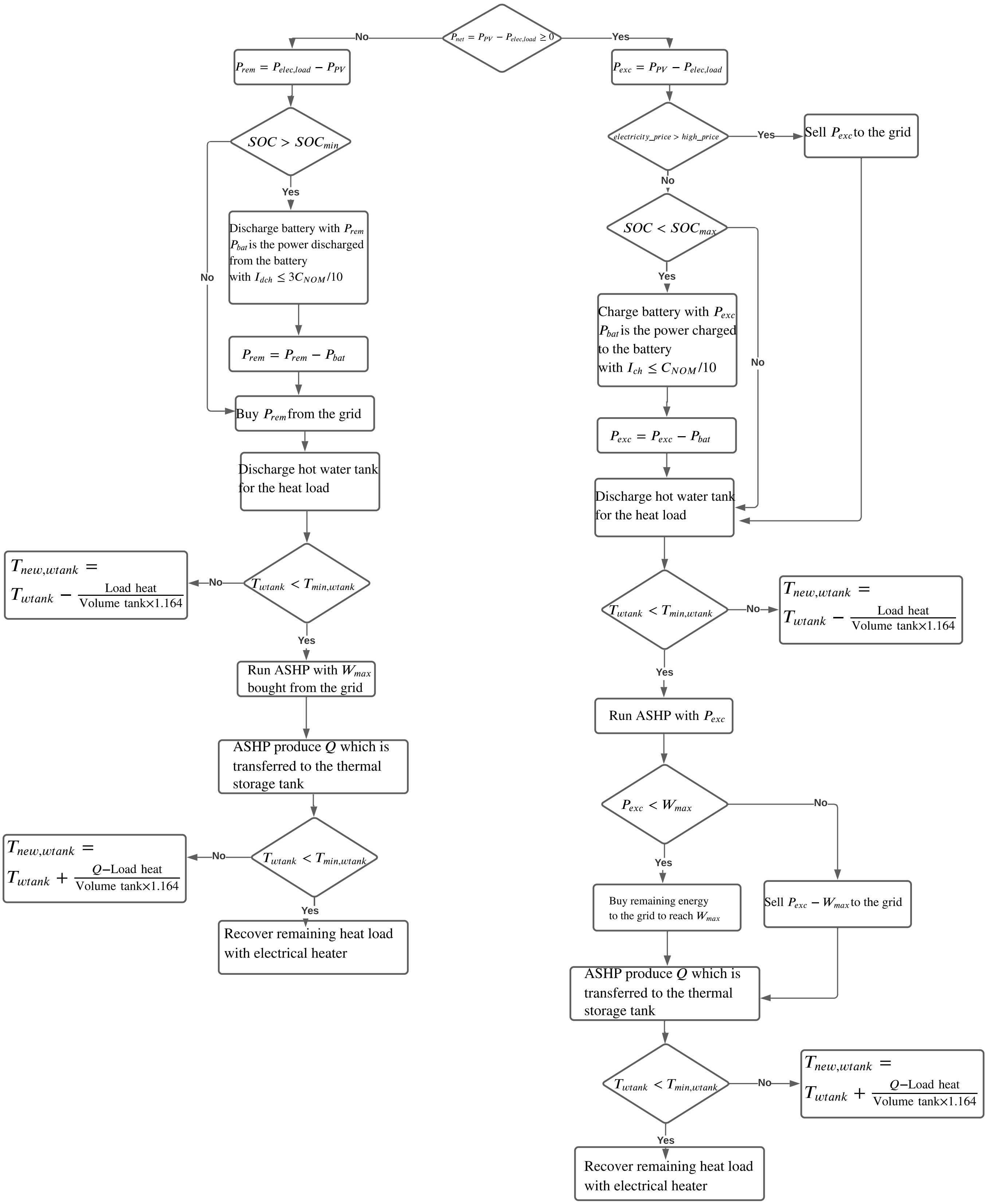

Figure 3.3: Decision tree for the grid selling strategy, a new design variable is included, $high\_price$. When the electricity price is higher than this threshold variable, the electricity excess is directly sold to the grid.

3.4 Temperature dependent heat pump strategy

This third strategy focuses on using the heat pump in the first place when there is PV power excess during cold temperatures. Looking at the climate and load data presented in the previous chapter, a negative correlation of -0.79 can be found between heat demand and ambient temperature. This strategy aims to understand if it is more efficient in a techno-economic way to first use the heat pump and then the battery with the power excess during cold temperatures. To do so, a new design variable, $critical\_temp$, is implemented in the framework. The strategy operates as follows: when the power generated by the PV array is higher than the demand, if the ambient temperature (temp_amb) is lower than the threshold temperature $critical\_temp$, the heat pump first uses the power surplus and then the battery stack if any power is left over. Otherwise, the reference operation is followed as explained in Section 3.1.

The decision tree of this strategy is illustrated in Figure 3.4.

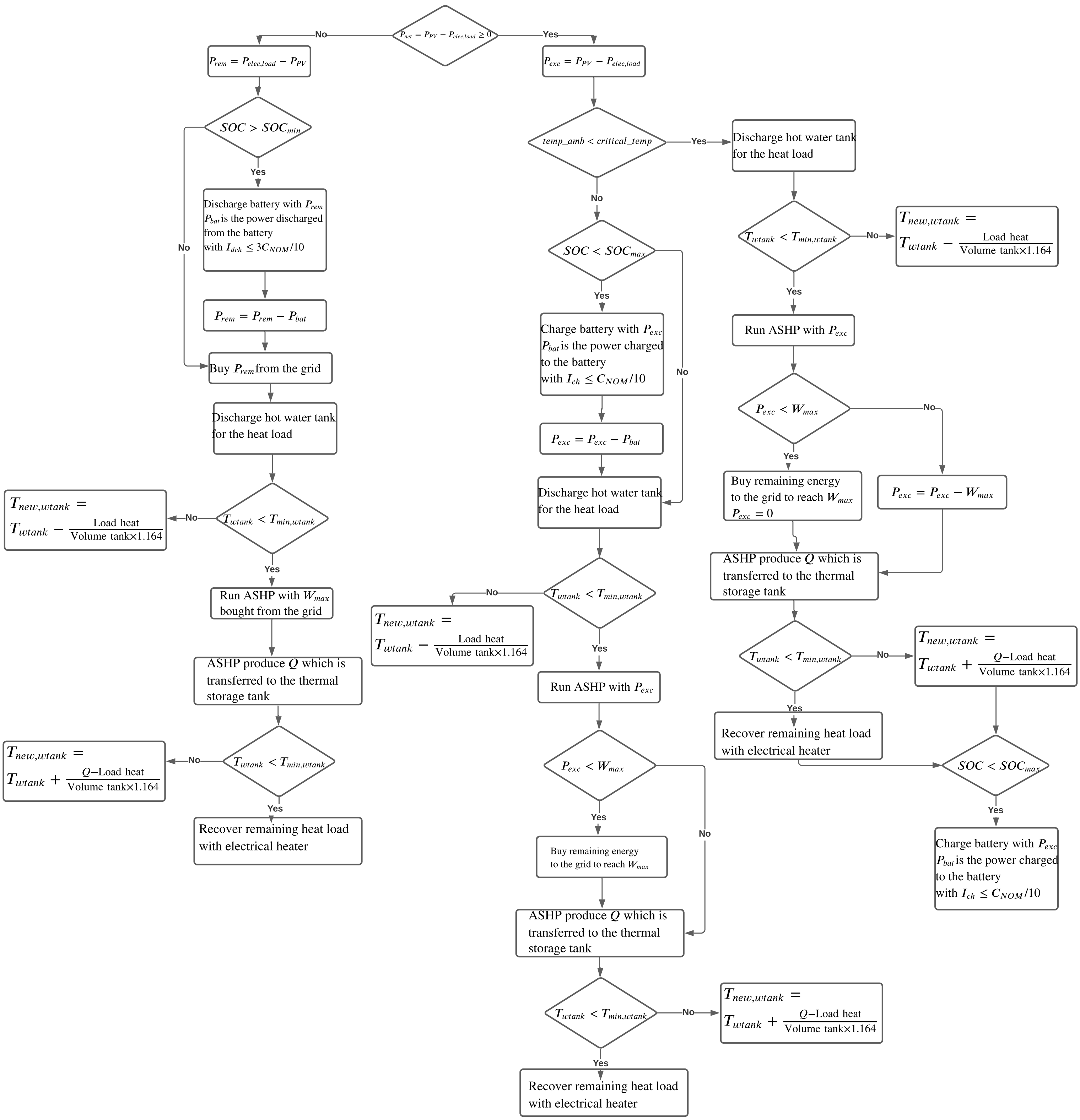

Figure 3.4: Decision tree for the temperature dependent heat pump strategy, a new design variable is included, $critical\_temp$. When the ambient temperature is lower than this threshold variable, the heat pump first uses the electricity surplus.

3.5 Partially charging strategy

This fourth strategy focuses on charging the battery partially with the PV power excess and using the ASHP with the remaining power. This strategy aims to understand if it is more efficient in a techno-economic way to charge the battery with a fixed percentage of the power excess and then use the ASHP with the remaining power. To do so, a new design variable, $percentage\_bat$, is implemented in the framework. The strategy operates as follows: when there is power excess, the battery is charged with $percentage\_bat \times \mathrm{P}_{\mathrm{net}}$ and the remaining power, $(100 - percentage\_bat) \times \mathrm{P}_{\mathrm{net}}$, is used by the ASHP. When there is a lack of power, the strategy follows the reference strategy explained in Section 3.1.

The decision tree of this strategy is illustrated in Figure 3.5.

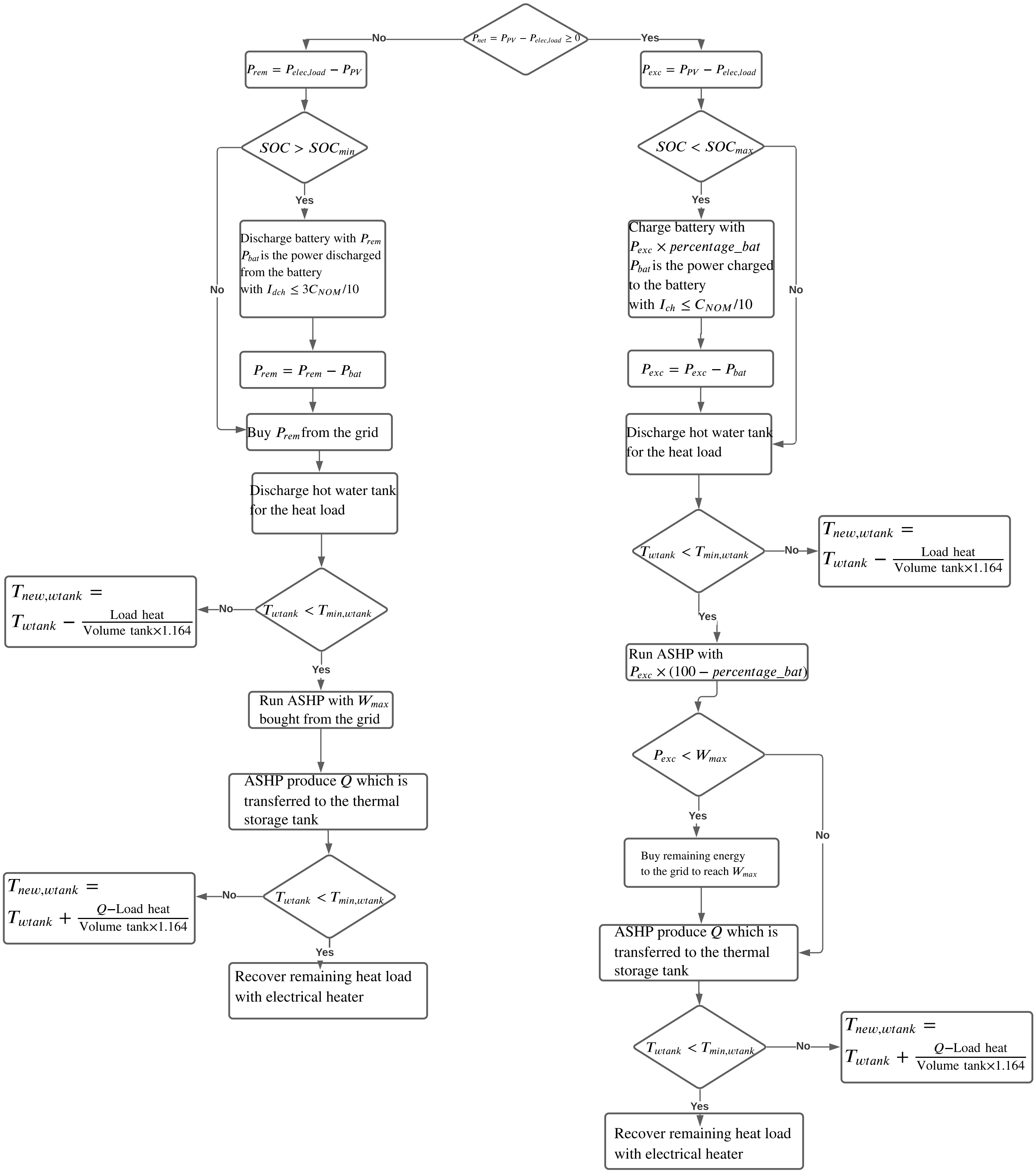

Figure 3.5: Decision tree for the partially charging strategy, a new design variable is included, $percentage\_bat$. The battery and heat pump both partially use the electricity excess.

3.6 Peak shaving strategy

This fifth strategy is based on the peak shaving operation. It uses the PV electricity source and battery storage to optimally charge, discharge, buy and sell electricity. To do so, two new design variables, low_power and $high\_power$, are implemented in the framework. At each hour the net power, $\mathrm{P_{net}} = (\mathrm{P_{PV}} - \mathrm{P_{elec,load}})$, is compared with the low and high power limit.

When $\mathrm{P_{net}}$ is positive and higher than $high\_power$, meaning that there is an electricity surplus and it is a peak hour, the electricity surplus is sold to the grid.

When $\mathrm{P_{net}}$ is negative and lower than low_power, meaning that there is a lack of energy and it is an off-peak hour, the missing electricity is bought to the grid.

When the system is not operating during peak or off-peak hours, the reference strategy is followed as explained in Section 3.1. The battery is either charged or discharged depending on the produced PV electricity and load.

The decision tree of this strategy is illustrated in Figure 3.6.

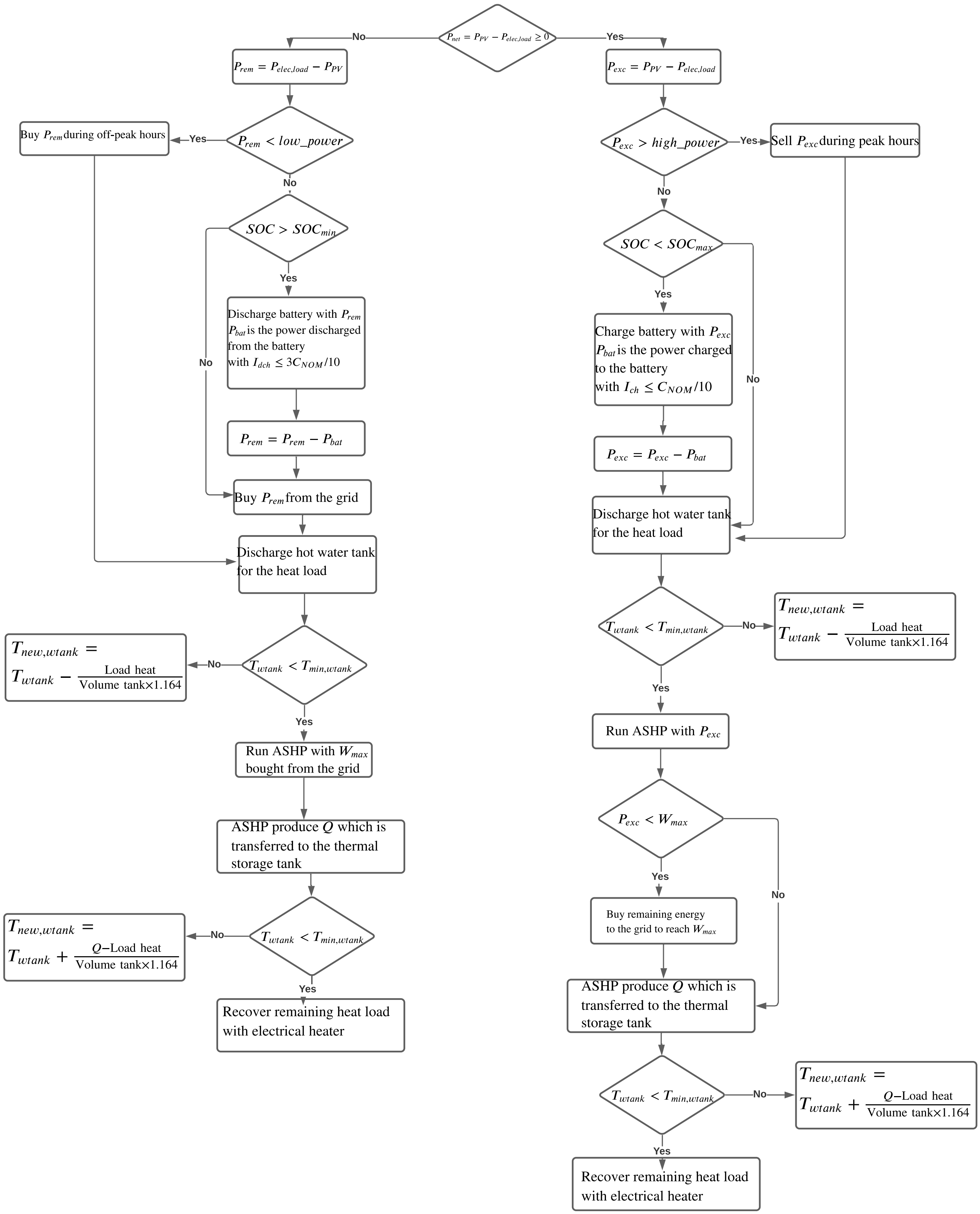

Figure 3.6: Decision tree for the peak shaving strategy, two new design variables are included, low_power and $high\_power$. When the electricity excess is higher than the high power limit, it is sold to the grid. Inversely, when the remaining power is lower than the low power limit, it is bought to the grid.

3.7 Forecast strategy

This sixth strategy focuses on a day-ahead forecast to optimally charge the battery to meet future demand. This strategy aims to understand if it is more efficient in a techno-economic way to charge the battery with 24 hours forecast. To do so, a 24-hour true forecast loop is created to evaluate the excess or lack of power generated by the PV array to meet the demand. The minimum wholesale price (min_elec_profile) in this 24-hour forecast loop is also obtained. The strategy operates as follows: it matches the reference strategy described in Section 3.1, but when the wholesale price of electricity is equal to the minimum of the next 24 hours, the battery is charged with the lack of energy calculated in the day ahead loop.

The decision tree of this strategy is illustrated in Figure 3.7.

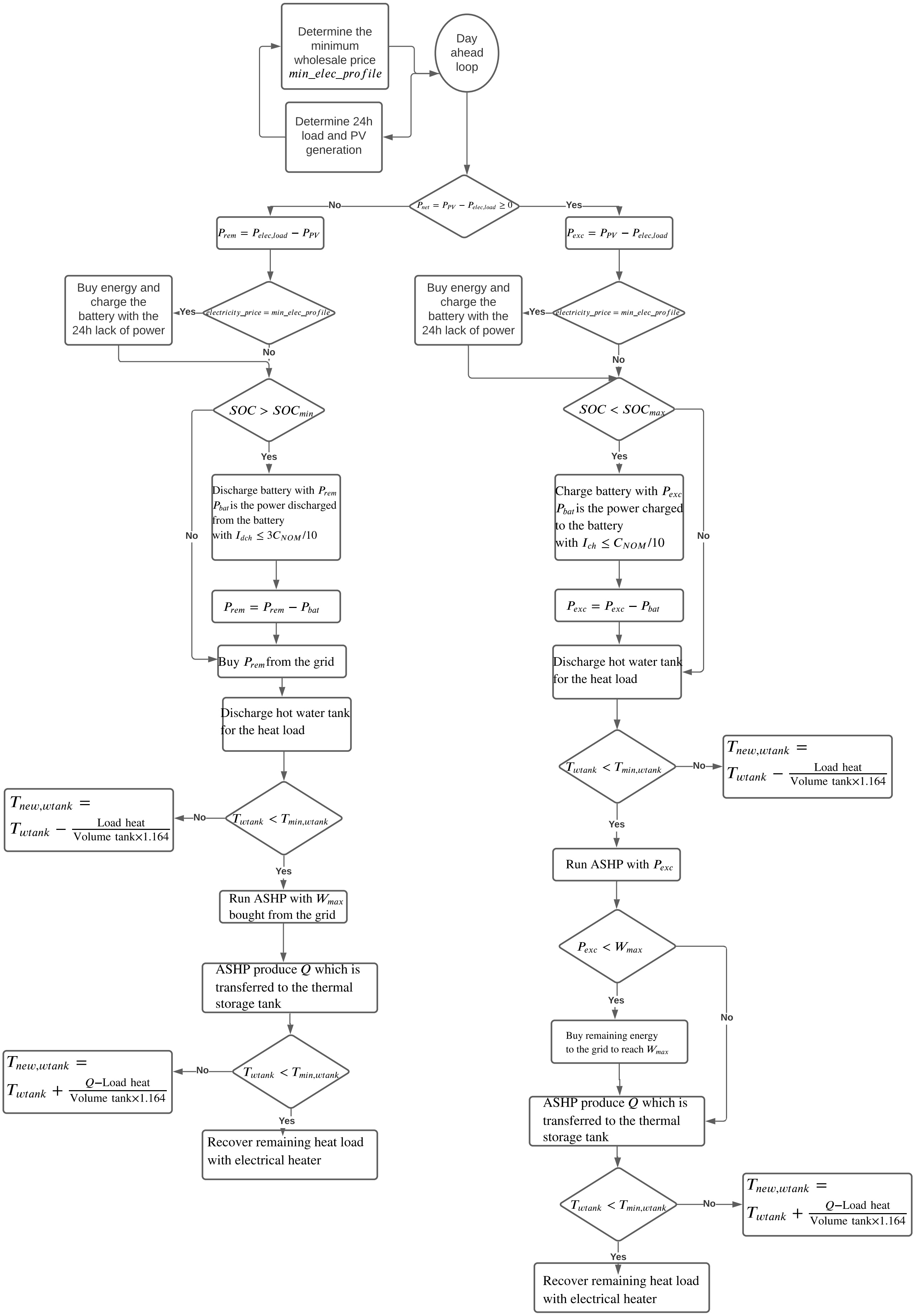

Figure 3.7: Decision tree for the forecast strategy, a new day ahead loop is made. It optimally charges the battery for the future lack of energy at low costs.

Chapter 4

Results and Discussion

This chapter presents the results of the robust design optimization. The interest is to find the designs with the optimized combination of the LCOX mean and the LCOX standard deviation. The RDO script uses the NSGA-II algorithm and the PCE method to optimize the PV - battery - heat pump - thermal storage tank model. The optimization is done according to the objectives of minimizing both the LCOX standard deviation and the LCOX mean. For each strategy, the Pareto set of the optimized designs is presented with a global sensitivity analysis on the uncertainties. Only the uncertainties having a Sobol' index higher than 0.05 will be shown. Subsequently, a general analysis between each strategy is performed. Finally, the stochastic performance of the chosen optimized designs is compared based on the Cumulative Distribution Function (CDF).

4.1 Robust Design Optimization and global sensitivity analysis on the different power management strategies

First, the results of the reference scenario will be shown. Afterwards, the results of the two strategies based on taking advantage of the variable wholesale price will be presented. Subsequently, the results of the two strategies linked to the heat pump use will be illustrated and finished by the results of the two strategies based on an overall different operation of the system.

4.1.1 Optimization of the reference strategy

Pareto front. After performing the RDO on the reference strategy, the result illustrates a trade-off between minimizing the LCOX mean and minimizing the LCOX standard deviation (Figure 4.1). The reduction in the standard deviation is more significant than the increase of the mean (13% against 5%).

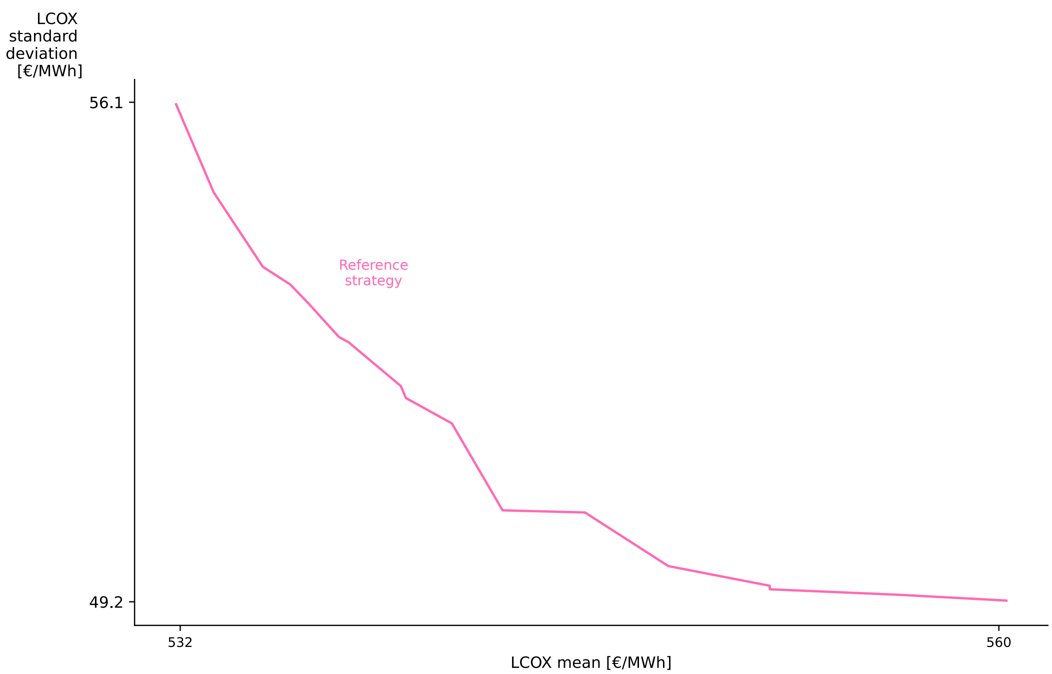

Figure 4.1: The Pareto front illustrates that a trade-off exists between minimizing the LCOX standard deviation and the LCOX mean. The gain in robustness is greater when shifting between the optimized mean and robust design mean.

Sobol' indices. Looking at the impact of the uncertainties on the LCOX standard deviation, Figure 4.2 illustrates the effects that each uncertainty can have on the designs. One can observe that the variation of the LCOX standard deviation is mainly due to the uncertainty on the electricity price and on the electricity load. Reducing the uncertainties around these parameters further helps to increase the system's robustness.

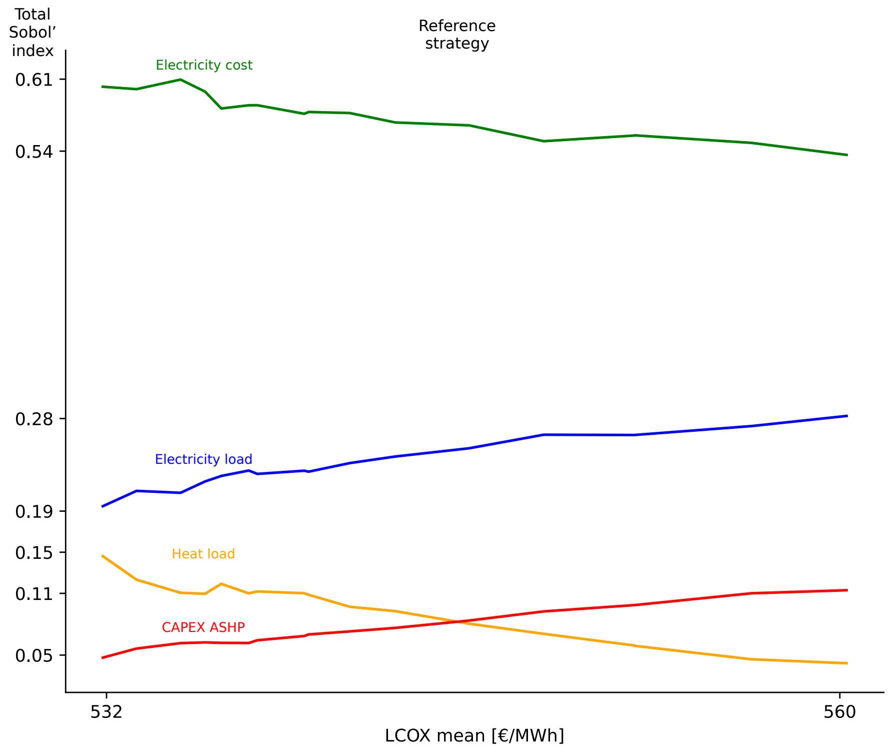

Figure 4.2: The Sobol' indices indicate that the uncertainty on the future electricity price is the dominant uncertainty for the LCOX. For the robust design, the uncertainty on the electricity price and on the electricity load play an important effect on the system's robustness. Reducing the uncertainties around these parameters further helps to improve the system's robustness.

System design variables capacities. To further clarify the results of the Pareto front and the Sobol' indices, a closer look at the design variables capacities is needed (Figure 4.3). The

LCOX mean increases with the battery and ASHP capacity. The gain in battery capacity decreases the effect of the uncertainty on the electricity price. The dependency on grid electricity is smaller thanks to more extensive energy storage. However, this increases the impact of the electricity demand uncertainty. Having more significant electricity storage means that the economic effectiveness depends on the match with the electricity demand. The gain in ASHP power decreases the effect of the uncertainty on the heat load but increases the uncertainty on the investment cost of the ASHP. Having a greater ASHP power allows producing a greater heat load to recover the heat demand.

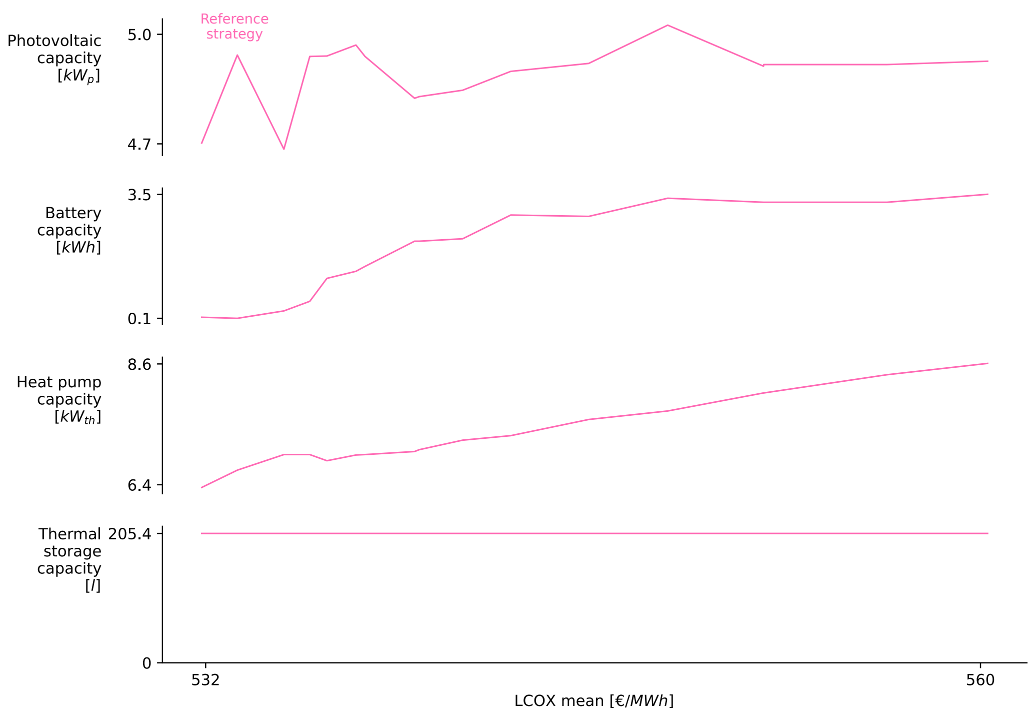

Figure 4.3: Reducing the LCOX standard deviation cost-efficiently is suggested by increasing the capacity of the battery stack and heat pump. This reduces the uncertainty linked to the electricity price and heat demand. However, it increases the uncertainty on the investment cost of the heat pump and on the electricity demand.

4.1.2 Optimization of the grid buying strategy

This strategy is the first one trying to take advantage of the variable wholesale price.

Pareto front. When performing the RDO on the grid buying strategy, the optimized LCOX standard deviation and the LCOX mean on the Pareto front are higher (up to 14% and 9% respectively, see Figure 4.4) than the reference case. This can be explained by the way the system operates under this strategy. As the system is buying energy from the grid to recover its load, it increases the costs related to the grid. This negatively impacts the LCOX.

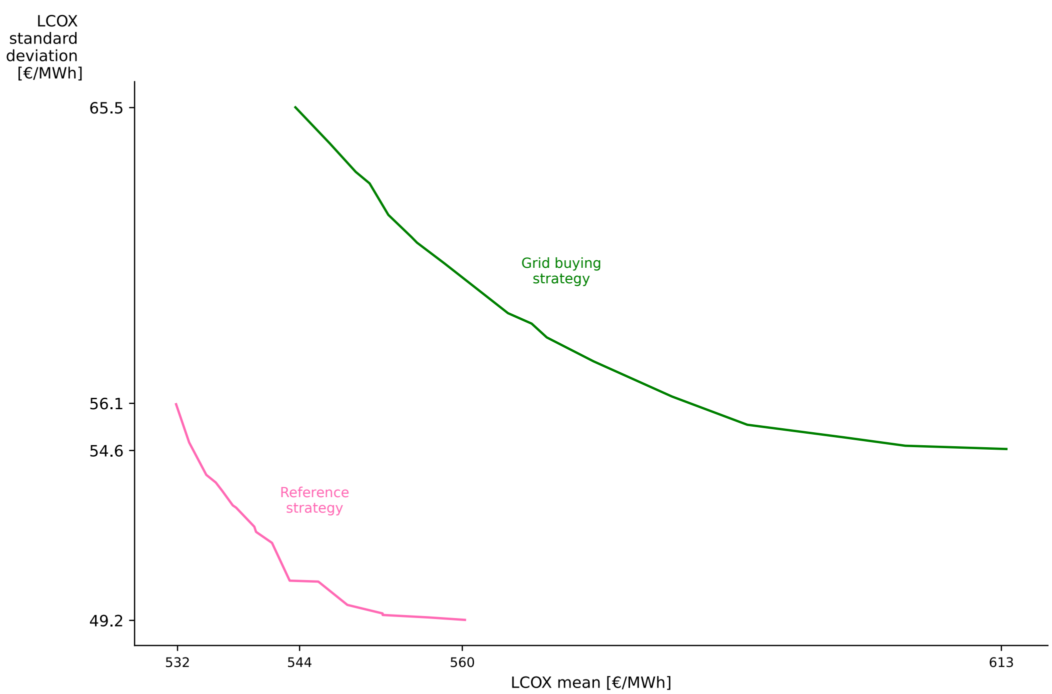

Figure 4.4: The Pareto front illustrates that a trade-off exists between minimizing the LCOX standard deviation and the LCOX mean. The Pareto front shows weaker results than the reference case. This is mainly because the system buys energy from the grid to recover its load, resulting in a higher LCOX.

Sobol' indices. The Sobol' indices represented in Figure 4.5 clearly illustrate that the variation of the LCOX standard deviation is mainly due to the uncertainty on the electricity price, electricity load and heat load. The value of the Sobol' index of the electricity cost is smaller than the reference case. However, the Sobol' index of the heat load is greater than the reference strategy. Reducing the uncertainties around these three parameters further helps to improve the system's robustness. One can observe that the uncertainty on the CAPEX of the ASHP is not present in the figure.

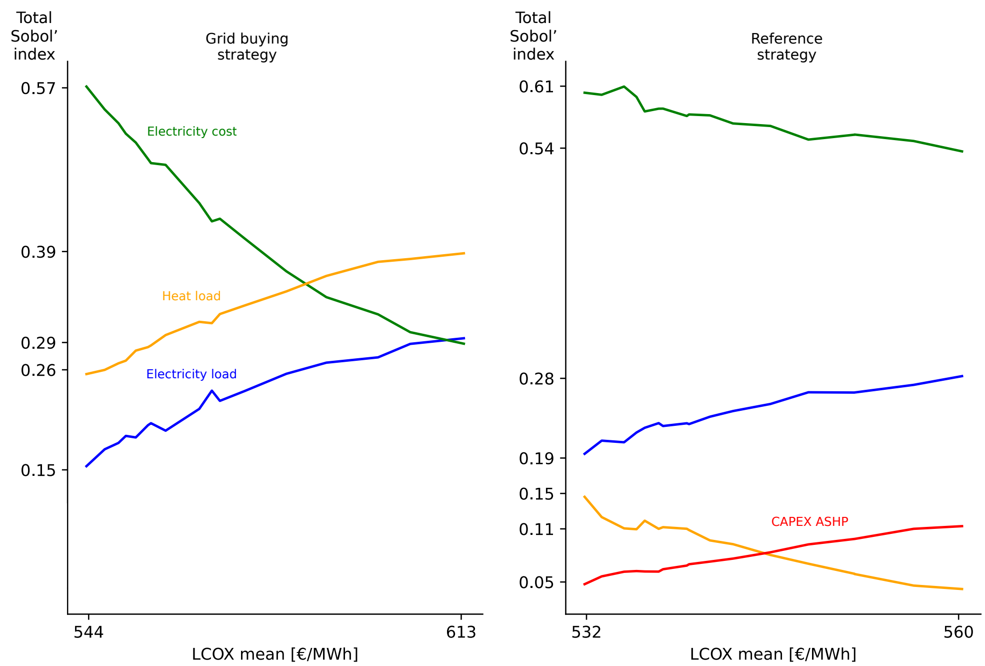

Figure 4.5: The Sobol' indices indicate that the uncertainty on the electricity price, electricity load and heat load are dominant for the LCOX. Reducing the uncertainties around these parameters further helps to improve the system's robustness.

System design variables capacities. To further clarify the results of the Pareto front and the Sobol' indices, a closer look at the design variables capacities is needed (Figure 4.6). As the LCOX mean increases, almost all design variables capacities stay constant. Moreover, they are all smaller than the reference case. This explains the previous results and is due to the working of the system, where it is buying energy to recover its needs. The system needs more minor capacities because it is mainly relying on the grid. The heat pump capacity being smaller (up to $4\mathrm{kW_{th}}$), the uncertainty on the CAPEX of the ASHP has little effect on the LCOX standard deviation. Subsequently, the lower PV and ASHP capacity increase the electricity demand and heat demand uncertainty, respectively. Having smaller electricity and heat sources are less able to produce enough energy to meet higher loads.

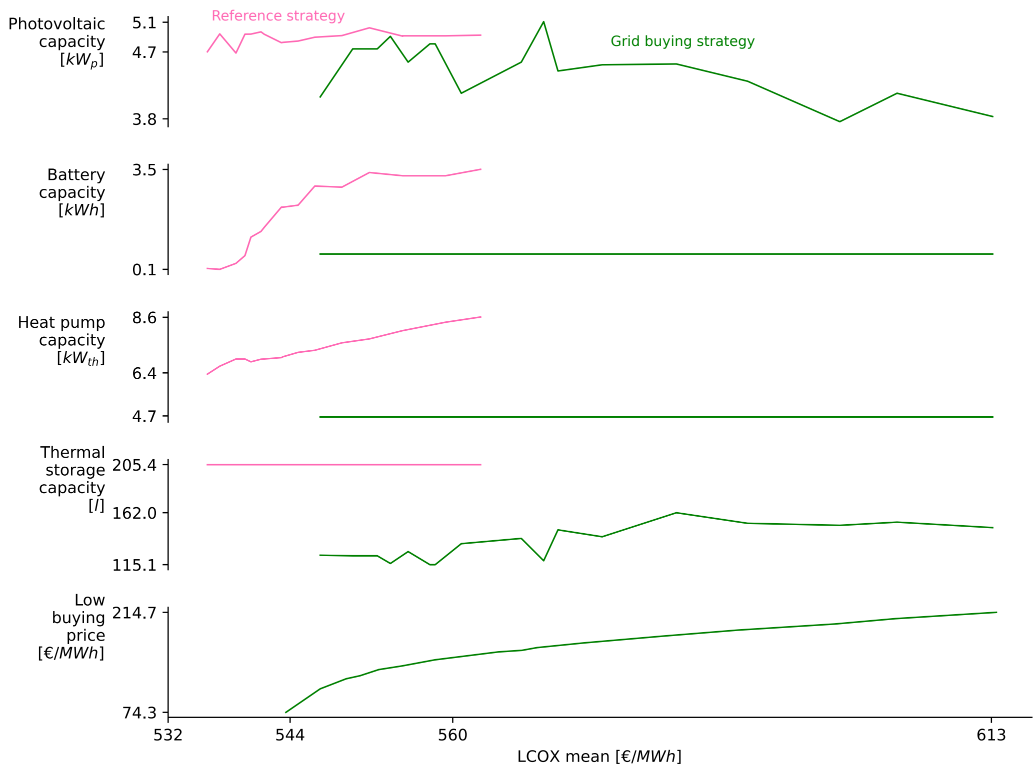

Figure 4.6: Reducing the LCOX standard deviation cost-efficiently is suggested by increasing the capacity of the thermal storage tank and the wholesale buying price. The system capacities of the photovoltaic array, battery stack, heat pump and thermal storage tank are smaller than the reference case, resulting in higher grid costs and a higher Sobol' index for the heat load. This explains the weaker results for the Pareto front.

4.1.3 Optimization of the grid selling strategy

This second strategy also takes advantage of the variable wholesale price by selling the electricity surplus to the grid.

Pareto front. When performing the RDO on the grid selling strategy, the optimized LCOX standard deviation and the LCOX mean on the Pareto front are lower (up to 20% and 13% respectively, see Figure 4.7) than the reference case. This can be explained by the way the system operates under this strategy. As the system can sell its energy surplus to the grid, it reduces its LCOX.

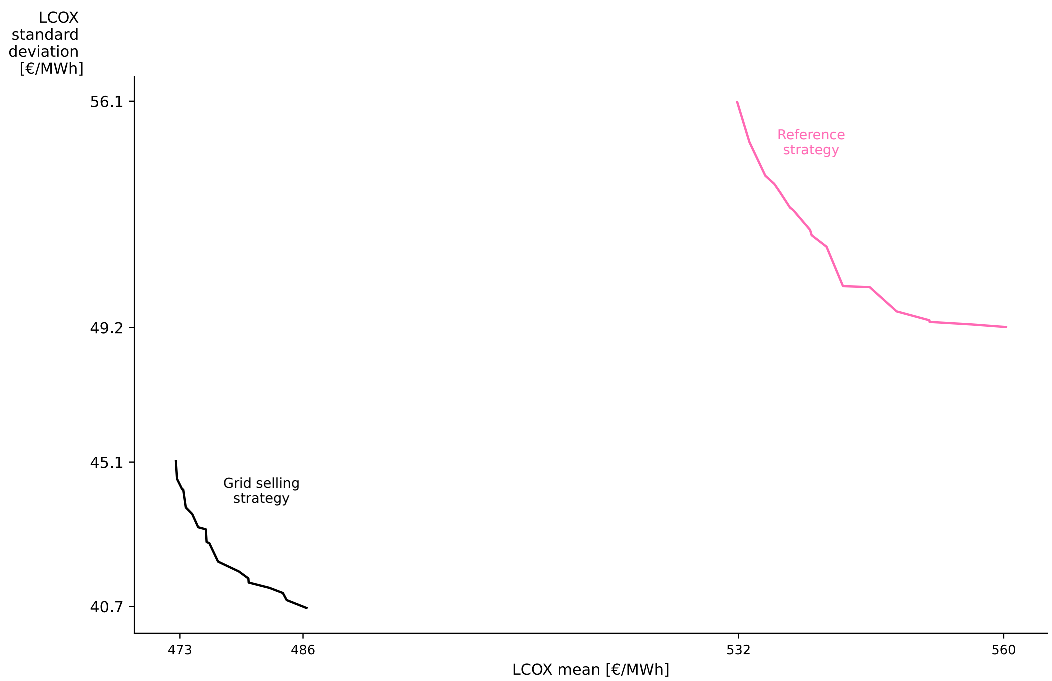

Figure 4.7: The Pareto front illustrates that a trade-off exists between minimizing the LCOX standard deviation and the LCOX mean. The Pareto front shows improved results than the reference strategy. This is mainly because the system sells its energy surplus resulting in a lower LCOX.

Sobol' indices. The Sobol' indices represented in Figure 4.8 clearly illustrate that the variation of the LCOX standard deviation is mainly due to the uncertainty on the electricity price and on the electricity load. Reducing the uncertainties around these two parameters further helps to improve the system's robustness. The value of the electricity cost Sobol' index is also lower than the reference strategy. This is possible because the system sells its electricity surplus to the grid, which counteracts the electricity price uncertainty when buying energy from the grid. This explains why the system under this strategy is more robust. Moreover, the CAPEX of the PV is included in the figure, meaning that this uncertainty can not be neglected.

System design variables capacities. To further clarify the results of the Pareto front and Sobol' indices, a closer look at the design variables capacities is needed (Figure 4.9). As observed, the system has a double PV capacity than the reference scenario. This explains why the uncertainty on the CAPEX of the PV is included in the Sobol' indices. It is to be noted that the PV power design variable was constraint to a maximum value of 10 kW_p. The optimizer created designs with the maximum allowed PV power. It was achieving a significant surplus of energy in order to sell it directly to the grid. Moreover, the heat pump capacity is increasing with the LCOX mean. This reduces the uncertainty on the heat load but increases the uncertainty on the CAPEX of the ASHP. Having greater ASHP power allows meeting the heat demand more easily but enlarges the investment cost. Subsequently, the robust design has a greater battery capacity than the optimized mean design. This increases the uncertainty on the electricity load. Having greater electricity storage means that the economic effectiveness depends on the match with the electricity demand. However, the battery capacity of the system remains small. This shows that the system is taking advantage of selling its energy excess to the grid instead of storing it. In the end, this decreases the LCOX.

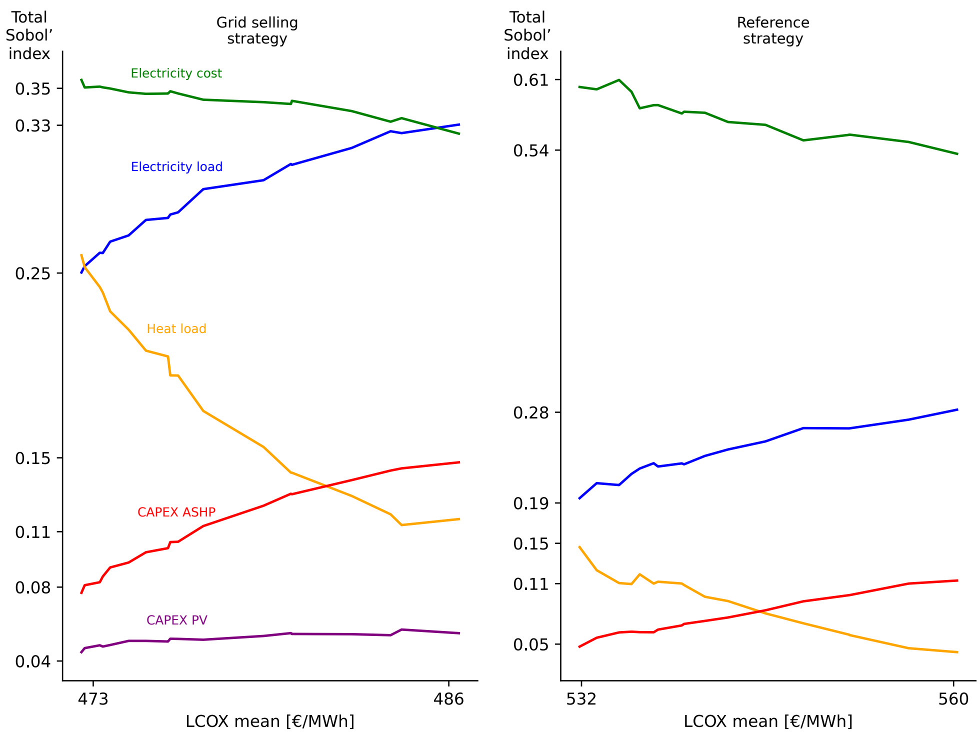

Figure 4.8: The Sobol' indices indicate that the uncertainty on the electricity price and on the electricity load are dominant for the LCOX. Reducing the uncertainties around these parameters further helps to improve the system's robustness. The CAPEX of the PV is also included and can not be neglected like for the reference case.

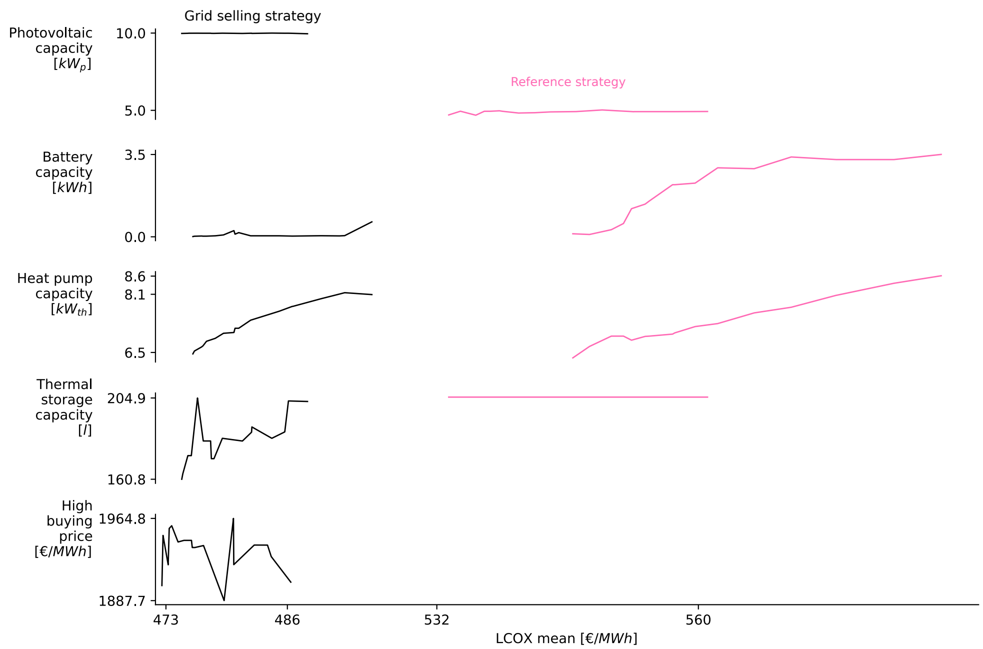

Figure 4.9: Reducing the LCOX standard deviation cost-efficiently is suggested by increasing the heat pump capacity. This reduces the uncertainty on the heat load but increases the uncertainty on the CAPEX of the ASHP. Moreover, the system has a double PV power than the reference case and almost no battery capacity. The system is taking advantage of selling its energy surplus to the grid to reduce its LCOX. This also explains why the Sobol' index of the CAPEX of the PV is included in the analysis.

4.1.4 Optimization of the temperature dependent heat pump strategy

This strategy is one of the two strategies that tries to understand how to optimally use the heat pump and battery stack with the energy excess.

Pareto front. When performing the RDO on the temperature dependent heat pump strategy, the optimized LCOX standard deviation and the LCOX mean on the Pareto front are similar to the reference case (Figure 4.10). However, the range of the Pareto front is smaller. A closer look at the design capacities is needed to understand this result.

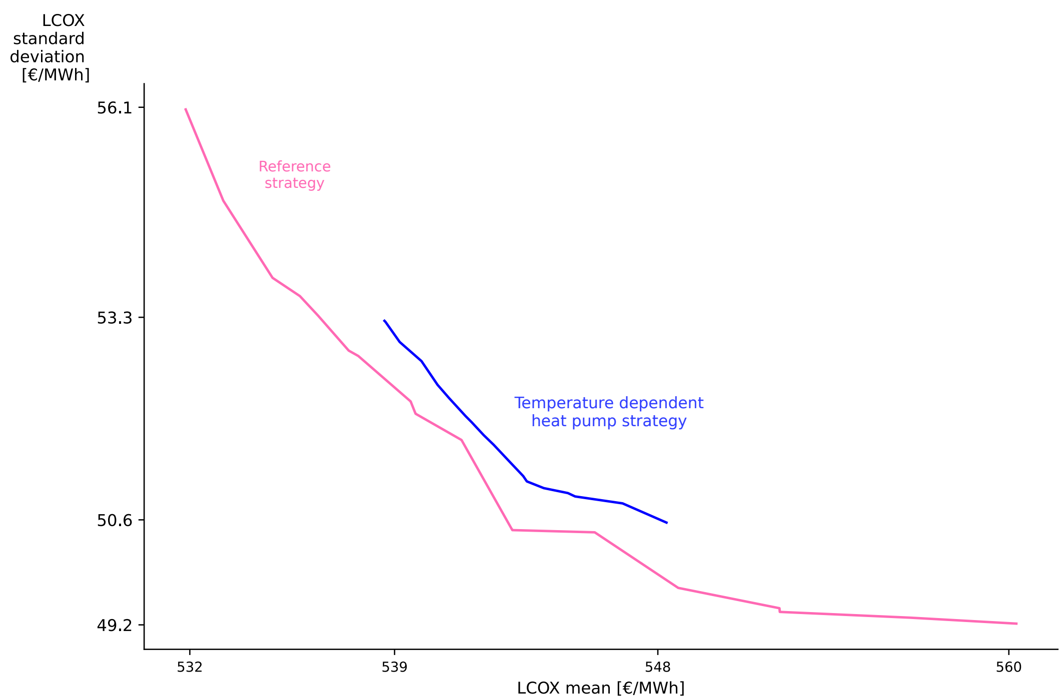

Figure 4.10: The Pareto front illustrates that a trade-off exists between minimizing the LCOX standard deviation and the LCOX mean. The Pareto front shows similar results to the reference case but with a smaller range of values. A closer look at the design capacities is needed in order to understand this result.

Sobol' indices. The Sobol' indices represented in Figure 4.11 clearly illustrate that the variation of the LCOX standard deviation is mainly due to the uncertainty on the electricity price and on the electricity load. Reducing the uncertainties around these parameters further helps to increase the system's robustness. Moreover, the uncertainties on the heat load and CAPEX of the ASHP are staying constant with the LCOX mean.

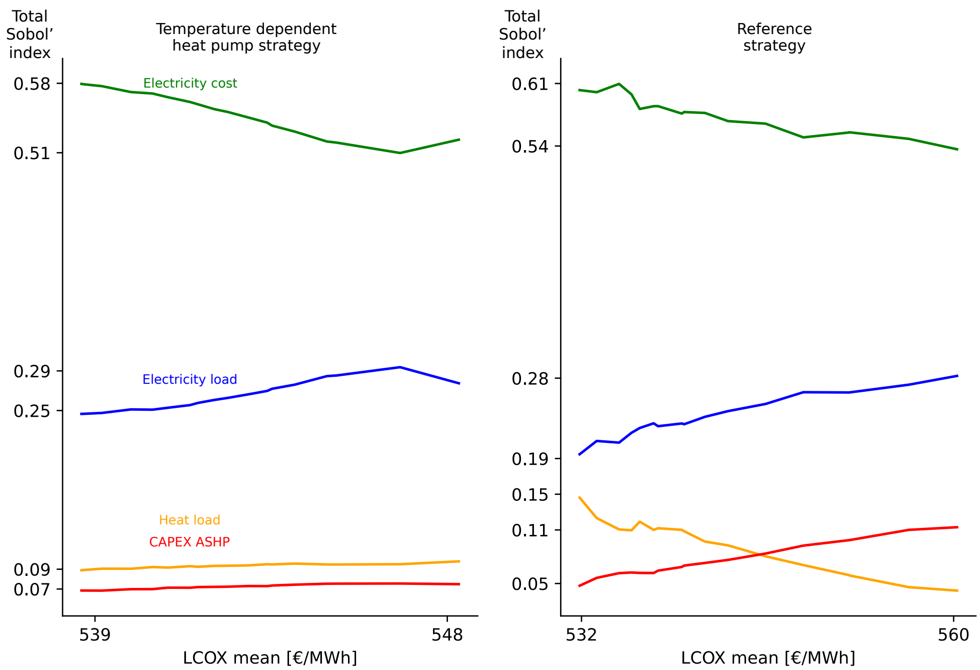

Figure 4.11: The Sobol' indices indicate that the uncertainty on the electricity price and on the electricity load are dominant for the LCOX. Reducing the uncertainties around these parameters further helps to improve the system's robustness. The uncertainty on the heat load and CAPEX of the ASHP stay constant with the LCOX mean.

System design variables capacities. To further clarify the results of the Pareto front and Sobol' indices, a closer look at the design variables capacities is needed (Figure 4.12).

As observed, the $critical\_temperature$ variable being equal to -3.9 degrees Celsius, with the available deterministic climate data, the system only follows this strategy less than 1% of the time. This explains why the Pareto front of this strategy is close to the reference case. Moreover, the heat pump and thermal storage tank capacities are staying constant, and so the uncertainty on the heat load and CAPEX of the ASHP. The battery capacity is increasing with the LCOX mean and the PV capacity is staying stable across each design except for the robust design. The gain in battery capacity decreases the impact of the uncertainty on the electricity price. The dependency on grid electricity is smaller thanks to larger energy storage. However, this increases the impact of the electricity demand uncertainty. Having greater electricity storage means that the economic effectiveness depends on the match with the electricity demand. Subsequently, the thermal storage tank is varying a lot. Its cost over the system's lifetime is low compared to the other components. The thermal storage tank is the least-impacting variable on the LCOX. The optimizer does not spend the most effort on tuning this variable and the variation between two points does not impact much the LCOX. Finally, most of component capacities being constant (i.e. only the battery capacity is increasing with the LCOX mean) explains well why the Pareto front has a lower range of values. The small range is only due to the increase in value of the battery capacity. Increasing the battery capacity lowers the LCOX standard deviation and increases the LCOX mean, but its effect is limited on the Pareto front.

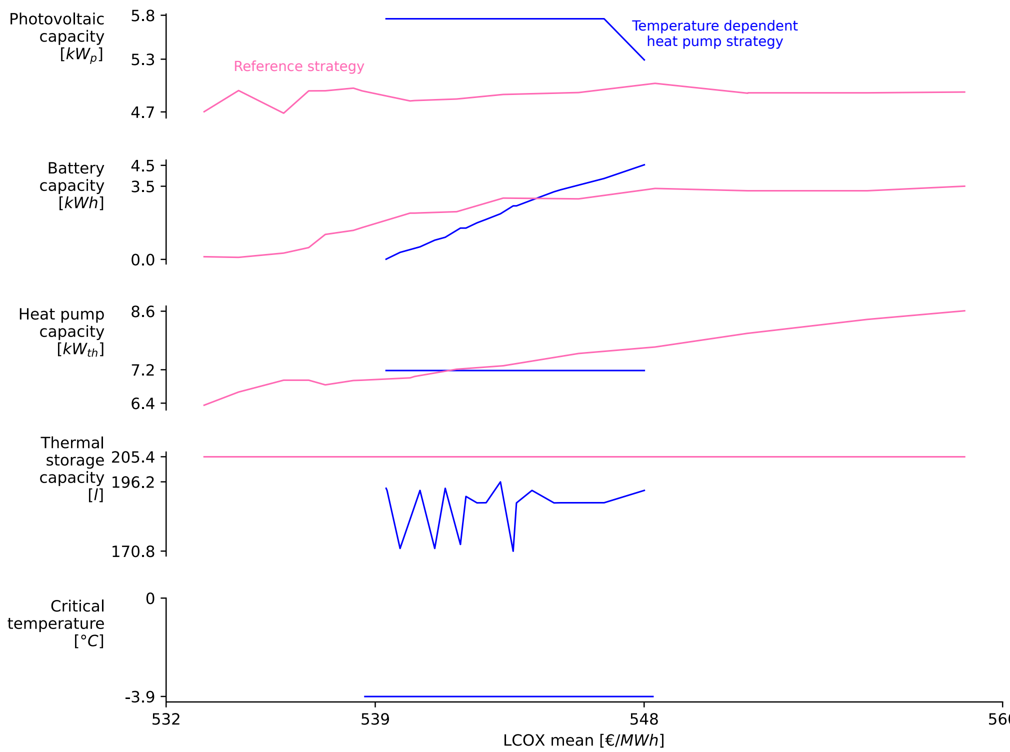

Figure 4.12: The $critical\_temperature$ being equal to -3.9 degrees Celsius, the system follows this strategy less than 1% of the time. Moreover, the heat pump and thermal storage tank capacities are constant, so the uncertainties on the heat load and on the CAPEX of the ASHP remain stable with the LCOX mean. The gain of the battery capacity with the LCOX mean decreases the electricity load uncertainty and increases the electricity cost uncertainty.

4.1.5 Optimization of the partially charging strategy

This fifth strategy is the last one that tries to understand how to optimally use the heat pump and battery stack with the energy surplus.

Pareto front. When performing the RDO on the partially charging strategy, the optimized LCOX standard deviation and the LCOX mean on the Pareto front are similar to the reference case (Figure 4.13). However, the range of the Pareto front is smaller. A closer look at the design capacities is needed to understand this result.

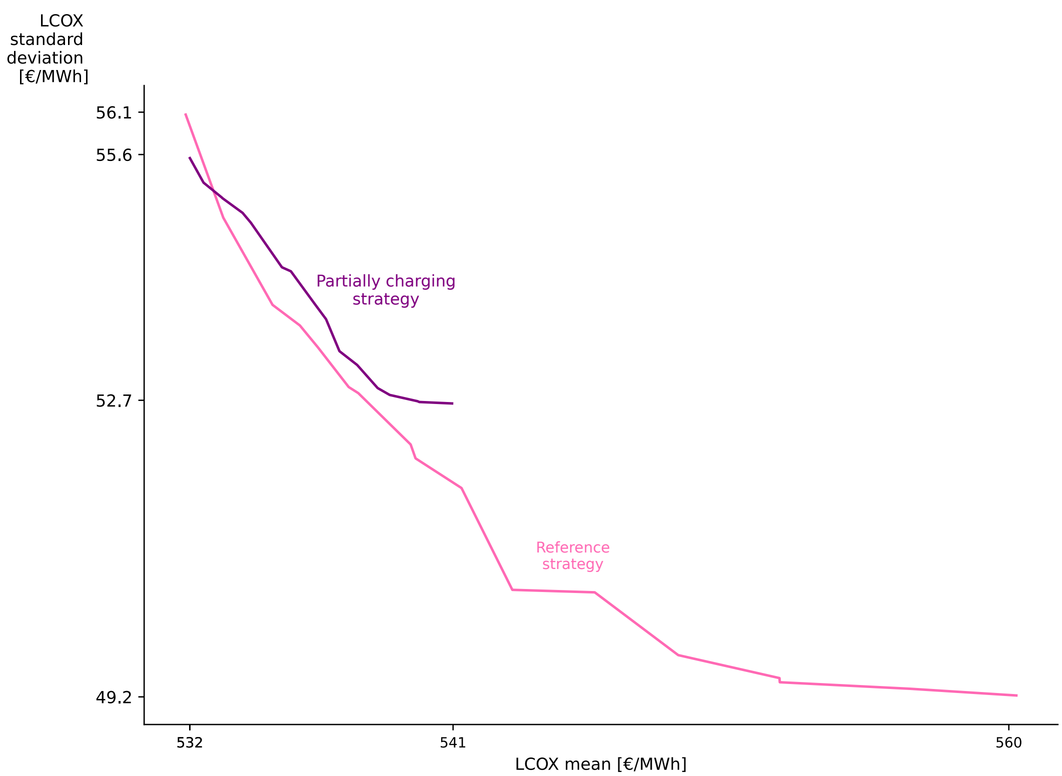

Figure 4.13: The Pareto front illustrates that a trade-off exists between minimizing the LCOX standard deviation and the LCOX mean. The Pareto front shows similar results to the reference case but with a smaller range of values. A closer look at the design capacities is needed to understand this result.

Sobol' indices. The Sobol' indices represented in Figure 4.14 clearly illustrate that the variation of the LCOX standard deviation is mainly due to the uncertainty on the electricity price. Reducing this uncertainty further helps to improve the system's robustness. Moreover, this strategy achieves a similar result for the Sobol' index of the electricity cost and smaller results for the Sobol' index of the electricity load and CAPEX of the ASHP. On the contrary, the uncertainty on the heat load is more significant than in the reference case.

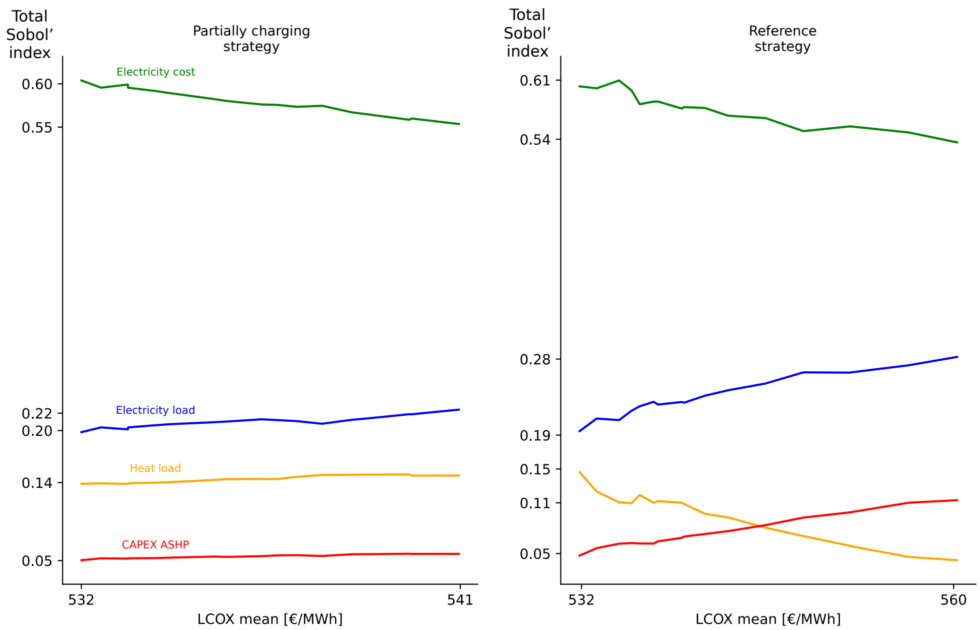

Figure 4.14: The Sobol' indices indicate that the uncertainty on the electricity price is dominant for the LCOX. Reducing the uncertainty around this parameter further helps to improve the system's robustness. The uncertainty on the electricity load, heat load and CAPEX of the ASHP stays constant with the LCOX mean.

System design variables capacities To further clarify the results of the Pareto front and Sobol' indices, a closer look at the design variables capacities is needed (Figure 4.15).

As observed, the $percentage\_bat$ design variable being consistently higher than 88%, the energy excess is mainly going to the battery. This explains why the Pareto front was so close to the reference case. Moreover, the heat pump and thermal storage tank capacities are staying constant with the LCOX mean. The uncertainty on the heat load and on the CAPEX of the ASHP will also remain steady with the LCOX mean. These capacities are also smaller than the reference case, resulting in a higher Sobol' index for the heat load and a smaller Sobol' index for the CAPEX of the ASHP than the reference strategy. Subsequently, the gain in battery capacity decreases the impact of the uncertainty on the electricity price. The dependency on grid electricity is smaller thanks to more extensive energy storage. However, this increases the impact of the electricity demand uncertainty. Having greater electricity storage means that the economic effectiveness depends on the match with the electricity demand. Finally, most of the component capacities being constant (i.e. only the battery capacity is increasing with the LCOX mean) explains well why the Pareto front has a lower range of values. The small range is only due to the increase in value of the battery capacity. Increasing the battery capacity lowers the LCOX standard deviation and increases the LCOX mean, but its effect is limited on the Pareto front.

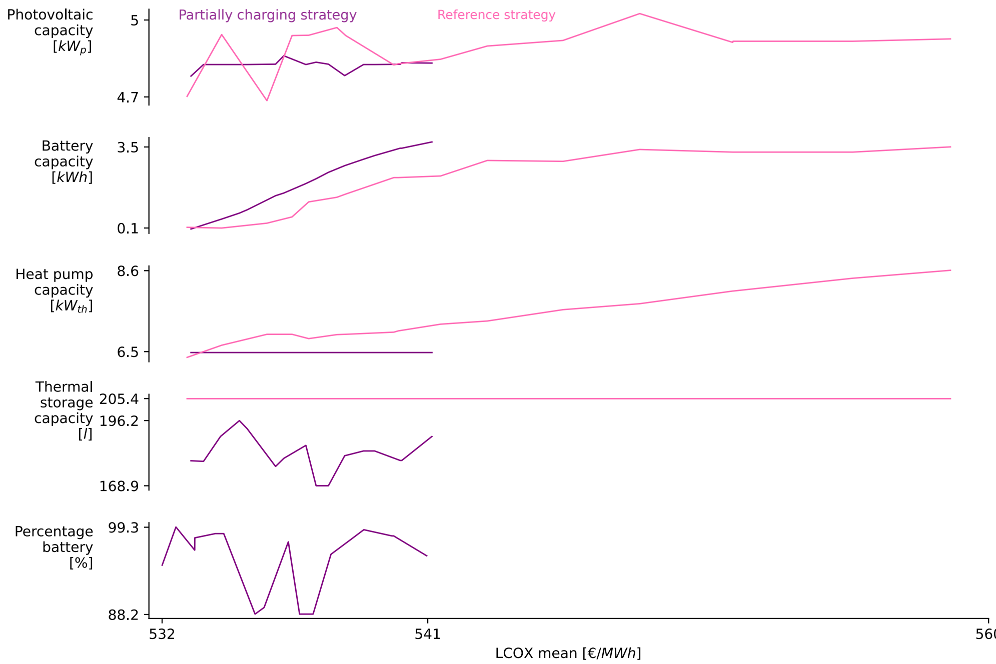

Figure 4.15: Reducing the LCOX standard deviation cost-efficiently is suggested by giving the major part of the electricity surplus to the battery and by increasing the battery capacity. The constant ASHP capacity explains why the Sobol' indices of the heat load and CAPEX of the ASHP stay constant with the LCOX mean.

4.1.6 Optimization of the peak shaving strategy

This strategy and the next one will be the two strategies having an overall different system operation.

Pareto front. When performing the RDO on the peak shaving strategy, the optimized LCOX standard deviation and the LCOX mean on the Pareto front are lower (up to 1.2% and 1.8% respectively, see Figure 4.16) than the reference case. This can be explained by the way the system operates under this strategy. The system is selling its energy surplus during peak hours and buying power during off-peak hours, which results in better performances for the LCOX.

Sobol' indices. The Sobol' indices represented in Figure 4.17 clearly illustrate that the variation of the LCOX standard deviation is mainly due to the uncertainty on the electricity price and on the electricity load. Reducing the uncertainties around these two parameters further helps to improve the system's robustness. The values of the Sobol' indices are similar to the reference strategy. Some minor variations are present, an analysis of the system capacities is needed to understand these results.

System design variables capacities. To further clarify the results of the Pareto front and Sobol' indices, a closer look at the design variables capacities is needed (Figure 4.18). One can observe that battery and heat pump capacity are similar to the reference case. This explains the similarities for the Sobol' indices for the heat load and CAPEX of the ASHP. The Sobol' index of the electricity cost is smaller than the reference case because, on the one hand, the greater PV array capacity and on the other hand, the system can sell its electricity surplus during peak hours. As the PV array is able to produce more energy, the system relies less on the grid. Moreover, the thermal storage tank has a smaller capacity, but its impact on the heat load is small. The thermal stored energy is negligible regarding the hourly heat demand. Subsequently, the low power limit and high power limit design variables explain why this strategy has better results regarding the Pareto front than the

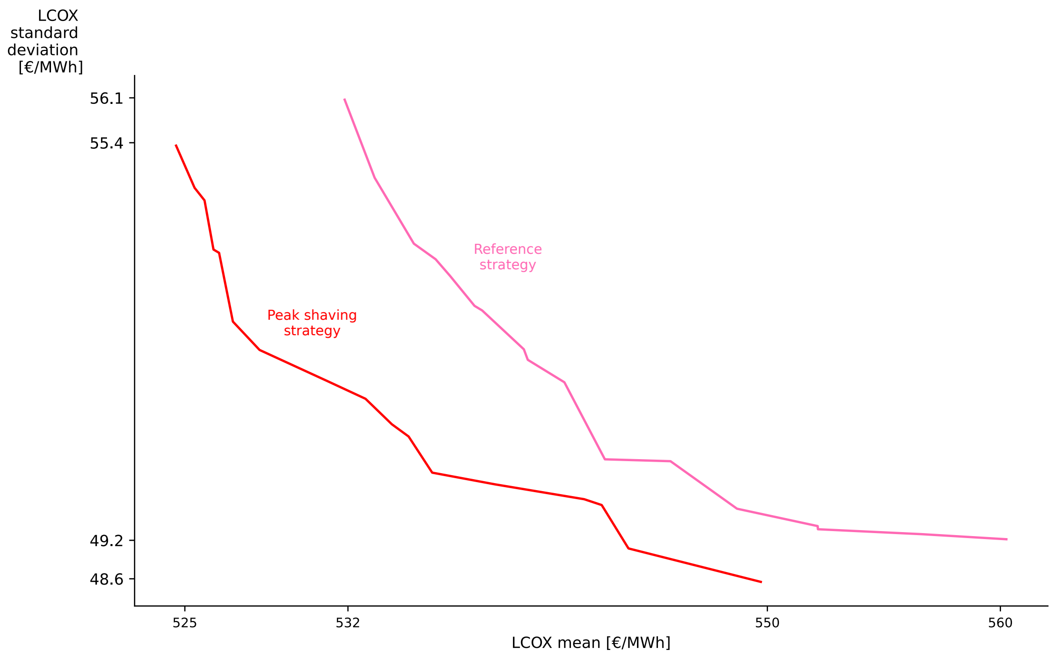

Figure 4.16: The Pareto front illustrates that a trade-off exists between minimizing the LCOX standard deviation and the LCOX mean. The Pareto front shows improved results than the reference strategy. This is mainly because the system sells its energy excess during peak hours to the grid and buys energy during the off-peak hours.

reference strategy. During peak hours, it can sell its energy surplus to the grid to profit from the possible high peak prices. During off-peak hours, it is buying energy from the grid instead of discharging the battery in order to take advantage of the possible low off-peak prices. It can be expected from this strategy to have an even better performance if there is a significant difference between peak and off-peak electricity prices. During a deterministic run of the robust design, the system was selling an energy excess 673 times during the peak hours and buying electricity 23 times from the grid. It shows well that the optimizer prefers to sell energy when it has an energy surplus and uses its own stored energy during lack of

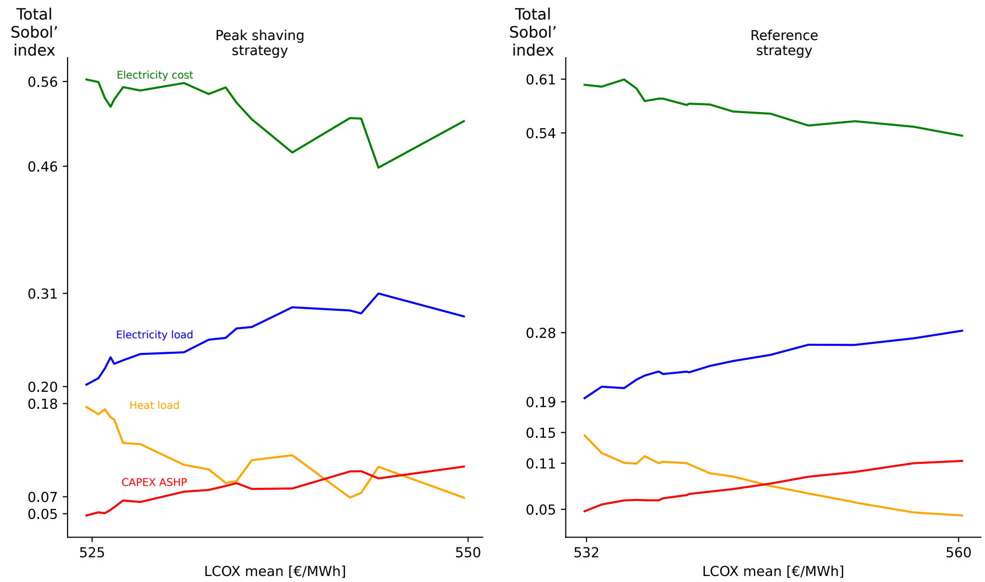

Figure 4.17: The Sobol' indices indicate that the uncertainty on the electricity price and on the electricity load are dominant for the LCOX. Reducing the uncertainties around these parameters further helps to improve the system's robustness. Moreover, the trends of these Sobol' indices are similar to the reference case.

power instead of buying it from the grid. This operation improves the LCOX. Finally, there is an overall increase in the battery, photovoltaic and heat pump capacity with the LCOX. However, there are some minor variations, which as a consequence, lead to the variations of the Sobol' indices.

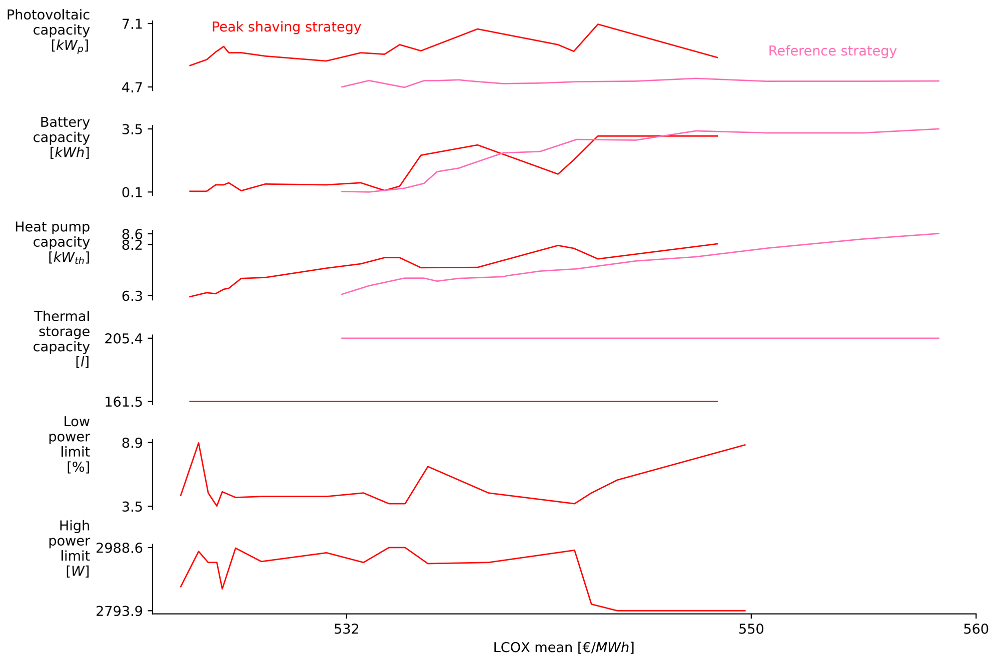

Figure 4.18: Reducing the LCOX standard deviation cost-efficiently is suggested by increasing the capacity of the battery stack, heat pump and thermal storage tank. This reduces the uncertainty linked to the electricity price and on the heat demand. However, it increases the uncertainty on the investment cost of the heat pump and on the electricity demand. Moreover, the lower and high power limit show how to operate the peak shaving strategy efficiently. Subsequently, the trends in the system capacities are similar to the reference case, this explains why the trends of the Sobol' indices were also similar to the reference strategy.

4.1.7 Optimization of the forecast strategy

The results of the forecast strategy are the last ones presented in this work.

Pareto front. When performing the RDO on the forecast strategy, the optimized LCOX standard deviation and the LCOX mean on the Pareto front are lower (up to 4.5% and 1.9% respectively, see Figure 4.19) than the reference case. This can be explained by the way the system operates under this strategy. As the system is making an exact day-ahead loop for the PV generation, demand and wholesale price, it can optimally charge the battery in advance with the lack of electricity for the coming hours and at the lowest price.

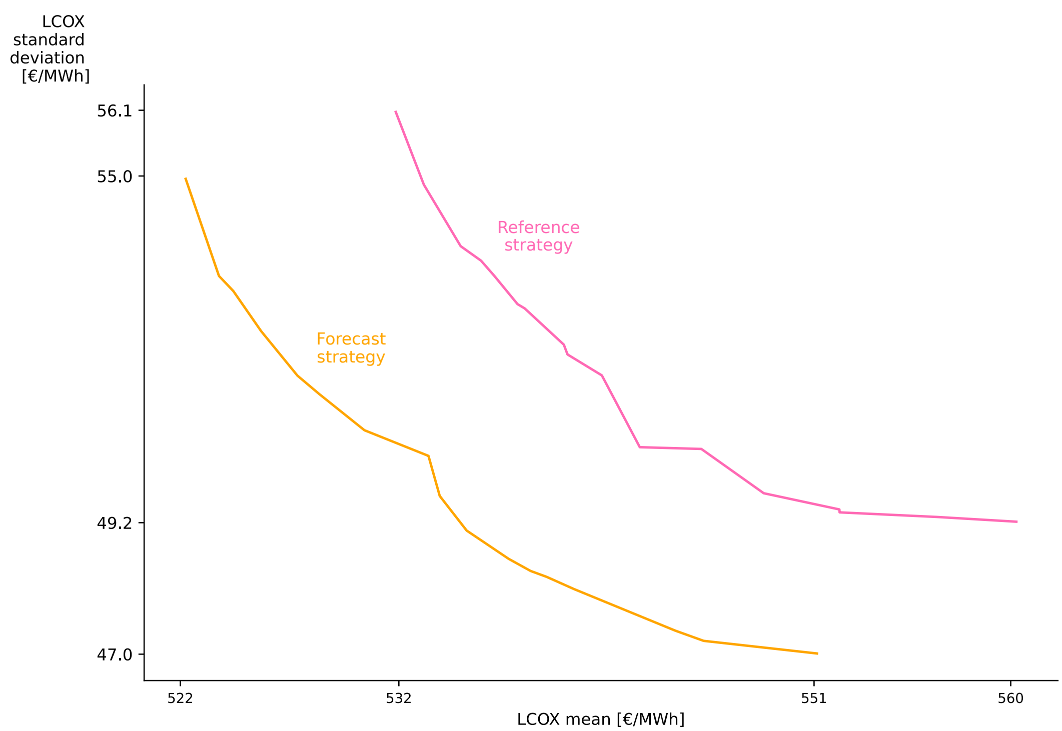

Figure 4.19: The Pareto front illustrates that a trade-off exists between minimizing the LCOX standard deviation and the LCOX mean. The Pareto front shows improved results than the reference strategy. This is mainly because the system is optimally charging its battery by a day-ahead forecast.

Sobol' indices. The Sobol' indices represented in Figure 4.20 clearly illustrate that the variation of the LCOX standard deviation is mainly due to the uncertainty on the electricity price and on the electricity load. The trends of the Sobol' indices of the uncertainties are similar to the reference case. Reducing the uncertainties around these two parameters further helps to improve the system's robustness.

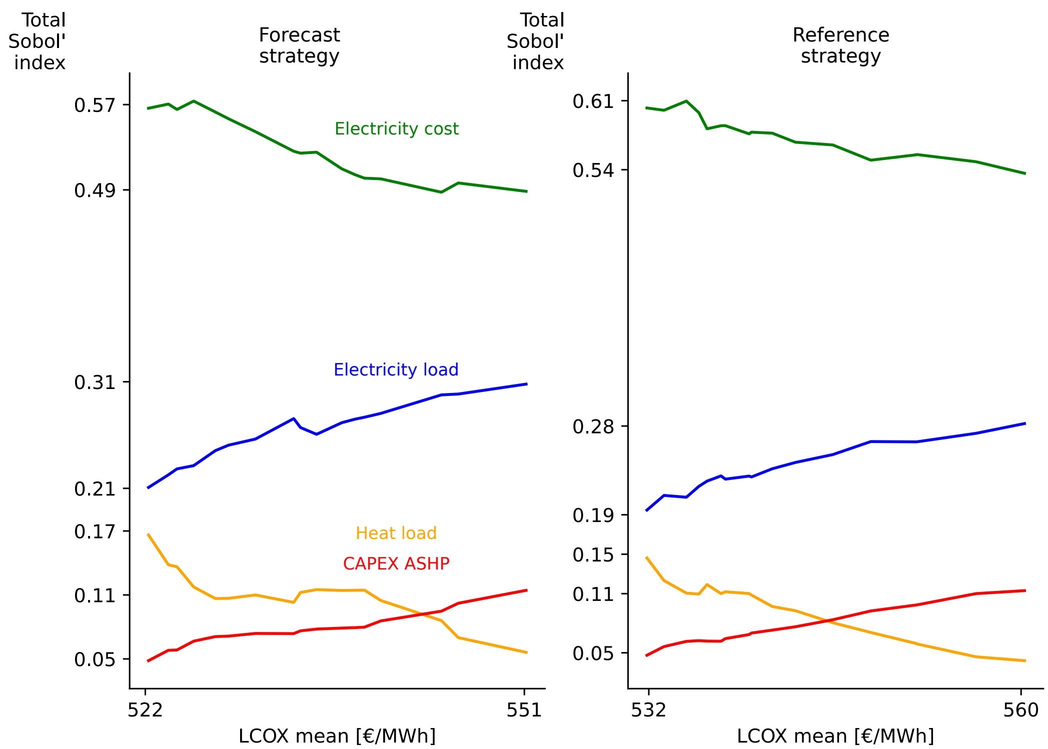

Figure 4.20: The Sobol' indices indicate that the uncertainty on the future electricity price is the dominant uncertainty for the LCOX. For the robust design, the uncertainty on the electricity price and on the electricity load play an important effect on the system's robustness. Reducing the uncertainties around these parameters further helps to improve the system's robustness.

System design variables capacities. To further clarify the results of the Pareto front and Sobol' indices, a closer look at the design variables capacities is needed (Figure 4.21).

Looking at Figure 4.21, one can observe that the system is increasing its robustness by having greater system capacities. Having greater battery and heat pump capacity reduces the Sobol' indices of the electricity cost and heat load but increases the Sobol' index of the electricity load. By having greater battery capacity, the system has less electricity to buy from the grid but having larger electricity storage means that the economic effectiveness depends on the match with the electricity demand. The increase in ASHP power decreases the impact of the uncertainty on the heat load but increases the investment cost uncertainty of the ASHP. Moreover, the battery of the system has a higher capacity than the reference case. This shows well that thanks to an optimal day-ahead loop, it can be interesting to store enough electricity for the coming hours at a low cost.

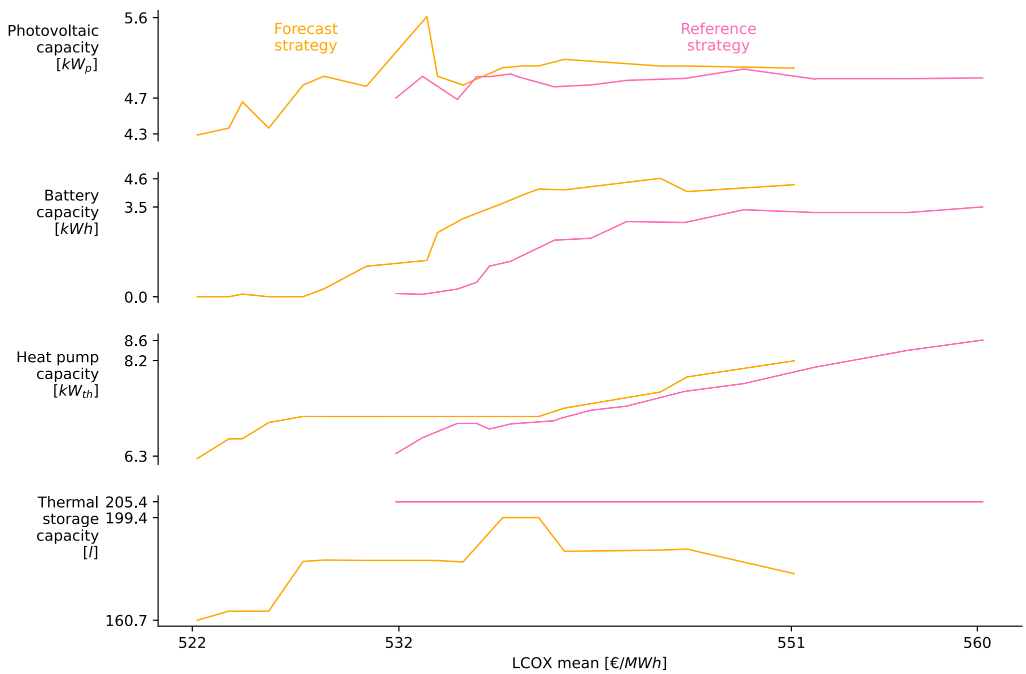

Figure 4.21: Reducing the LCOX standard deviation cost-efficiently is suggested by increasing all the system capacities. Moreover, the battery capacity is greater than the reference case. This shows well that thanks to an optimal day-ahead loop, it can be interesting to store enough electricity for the coming hours at a low cost.

4.2 General analysis of the performance of the power management strategies

In this subsection, the previous results are analyzed.

Pareto fronts. The different Pareto fronts related to each strategy are illustrated in Figure 4.22.

First, let's look at the two strategies trying to take advantage of the variable wholesale price, namely the grid buying and grid selling strategy. One can observe that they are distant from the other Pareto fronts. As discussed earlier, the grid selling strategy achieves the lowest LCOX standard deviation and the LCOX mean. This strategy achieves better performances because it is the only strategy which sells its energy surplus during all time of the day. Thus, this system was heaving the greatest PV array capacity but the smallest battery capacity because it maximizes its profit by selling the maximum amount of energy to the grid. Then, looking at the grid buying Pareto front, it shows the weakest results. This strategy often buys energy from the grid, increasing its LCOX mean and LCOX standard deviation by having high grid costs and uncertainties on the electricity cost and loads, respectively. The system had small component capacities and so was mainly relying on the grid. It can be concluded from these two strategies that selling its electricity excess to the grid is a great advantage for the household owner. Moreover, it is better to rely on its electricity production and storage components than buying directly from the grid.

Subsequently, one can observe that the two strategies trying to understand how to use the battery and heat pump optimally with the energy excess have similar results to the reference case. The temperature dependent heat pump strategy had a threshold temperature of -3.9 degrees Celsius, which was happening less than 1% of the time. The system mainly followed the reference strategy. Regarding the partially charging strategy, the energy surplus going to the battery was consistently greater than 88%. Thus, this strategy was also following mostly the reference case. It can be concluded from these two strategies that giving the priority of the battery on the energy surplus conducts to a better performance of the system in an exergy environment.

Finally, the two last strategies presented in this work were the peak shaving and forecast strategy. The two Pareto fronts are achieving better results than the reference case. The peak shaving strategy was operating differently during peak, regular and off-peak hours. During peak hours, it was selling its energy excess in order to take advantage of the possible high electricity prices. During off-peak hours, it was recovering its loads with the possible low prices. Outside these moments, the system was following the reference strategy. For the forecast strategy, it was optimally charging its battery at low costs with a day-ahead loop. Thanks to this forecast, the system knew which quantity of energy it had to buy to recover the load and to take advantage of an hour with low wholesale prices. By doing so, it could have smaller grid costs and the system had a greater battery capacity to store the bought energy. It can be concluded from these two strategies that having a more elaborated operation scheme, where it can either take advantage of the peak and off-peak hours or either make a day-ahead forecast, the system can achieve better results.

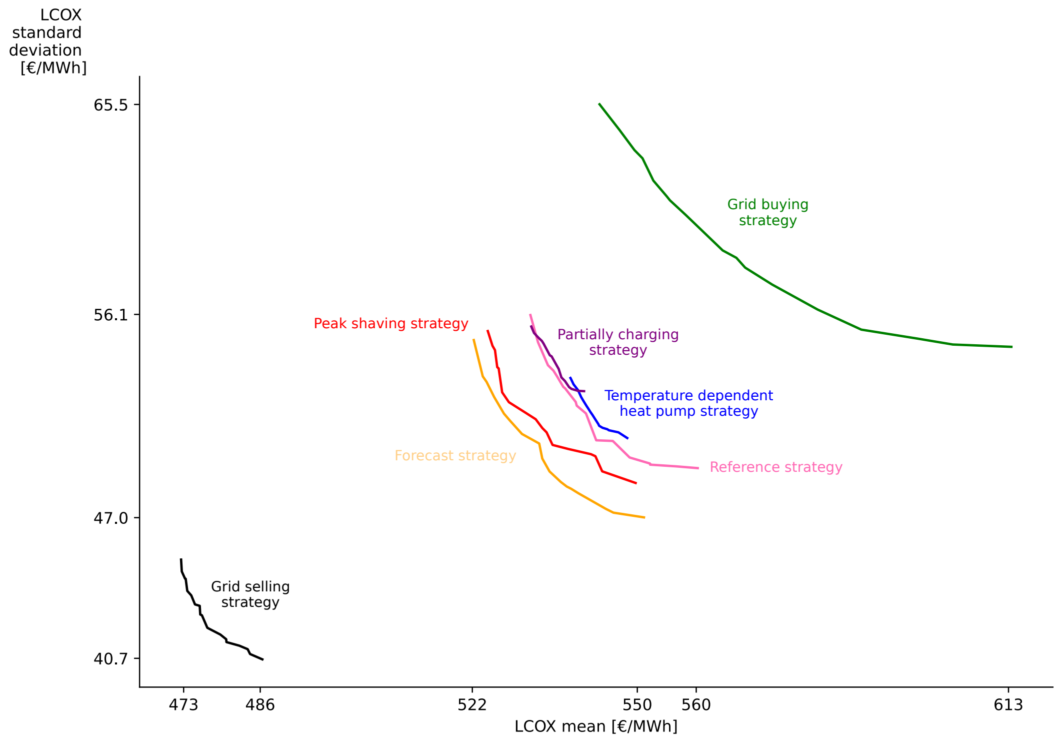

Figure 4.22: The Pareto fronts of all the strategies illustrate that a trade-off exists between minimizing the LCOX standard deviation and the LCOX mean. The grid selling strategy achieves the lowest LCOX standard deviation and the LCOX mean. The grid buying strategy achieves the highest LCOX standard deviation and the LCOX mean. The heat pump related strategies achieve similar results to the reference case due to the higher quality of electricity than heat. The two strategies having an overall different system operation (i.e. peak shaving and forecast strategy) achieves better results by either taking advantage of the peak and off-peak hours or either by making an optimal day-ahead loop where the battery is charged.

Sobol' indices Looking at Figure 4.23, the main Sobol' indices are represented for the robust designs of each strategy. One can observe that the uncertainty on the electricity cost and electricity load have the most impact on the LCOX standard deviation. The electricity

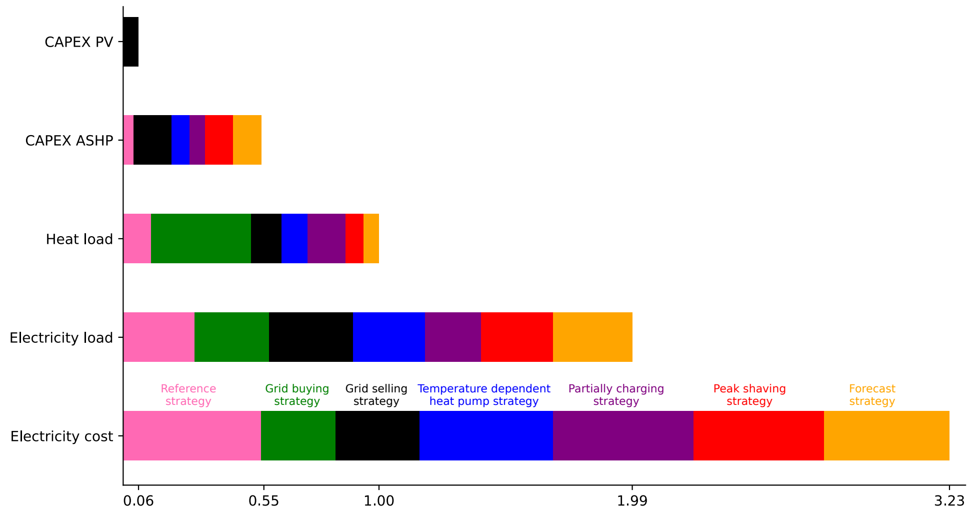

Figure 4.23: Stacked bar chart of the main uncertainties of the robust designs for the different strategies. The uncertainty on the electricity cost and electricity load have the greatest impact on the LCOX standard deviation. Reducing the uncertainty around these parameters further improves the system's robustness.

cost is the leading source for the LCOX standard deviation. It has a dominant effect on each strategy. Reducing the uncertainty around these parameters further helps to improve the standard deviation of the LCOX for all strategies. This means that once the future electricity mix is fixed, it is possible to have a more precise idea of the evolution of the electricity price. The electricity load depends on the prospective consumer behavior and loads (electric vehicle, connected objects, etc.). Subsequently, the uncertainties on the heat load and CAPEX of the ASHP also impact some strategies but less than the two previous ones. This is mainly due to the reduced weight of heat in an exergy environment due to the Carnot coefficient (see Equation 2.6). Finally, only the grid selling strategy has an impact of the CAPEX of the PV due to the great PV power.

4.3 Comparison of the stochastic performance

Due to the trade-off between minimizing the LCOX mean and minimizing the LCOX standard deviation, each design of each strategy out of the Pareto set carries an advantage in either average performance or robustness. To analyze the performance or robustness of each strategy, the Cumulative Density Function (CDF) is constructed for an optimal design for each strategy. To find these optimum designs, the knee point method is applied to each Pareto set of designs [56]. This method uses the minimum distance selection method in order to obtain the knee point. This point has the smallest distance from the utopia point. The utopia point is the point combining the smallest LCOX mean and smallest LCOX standard deviation from the Pareto set of designs. The optimum designs are shown in Figure 4.24.

The constructed CDFs for each optimal design car be found in Figure 4.25. Among the different strategies, the grid selling strategy achieves the highest probability that, in reality, the resulting LCOX over the lifetime will be lower than any predefined LCOX upper limit for the household. To illustrate the differences in each strategy, if the household owner predefines an LCOX upper limit of 550€/MWh, the forecast and peak shaving strategy provides a probability of 70% that the LCOX, in reality, will be below or equal to that upper limit (see Figure 4.25 below). Comparing it with the other strategies, it gives a probability of 62% for the partially charging strategy, temperature dependant heat pump and reference strategy (see Figure 4.25 middle). The grid selling and grid buying strategies have a probability of 95% and 55% respectively of being lower than this limit (see Figure 4.25 top). It can be concluded that the stochastic performance of the system can be improved with respect to the reference strategy in three ways. First, by being able to sell its surplus of energy to the grid. This allows reducing its grid costs and uncertainty related to the electricity cost, leading to a smaller LCOX. Second, by having a different operation during peak, regular and off-peak hours. The system is taking profit from selling its surplus of energy or buying energy from the grid at optimal hours. This strategy can be even more interesting if there is a significant difference between peak and off-peak electricity prices. Finally, by doing an optimal

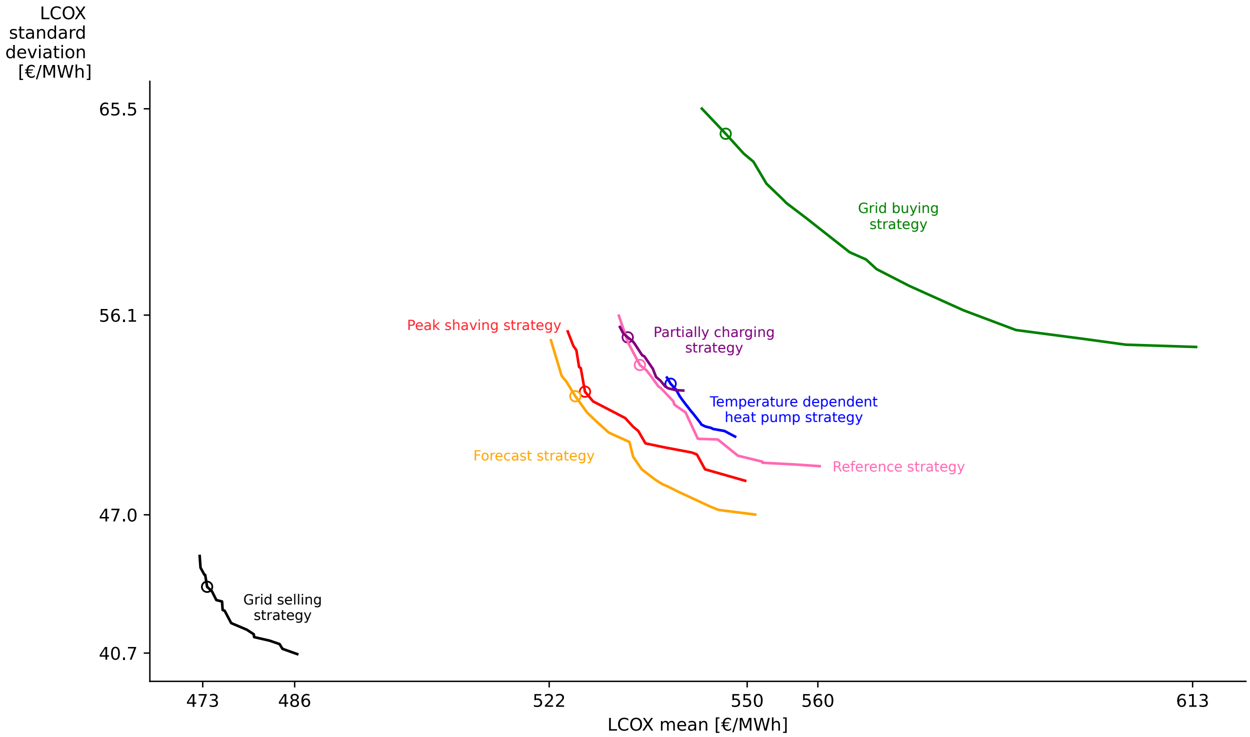

Figure 4.24: The optimum designs of each designs are highlighted on the different Pareto fronts. Each designs is the closest from the utopia point from his strategy.

day-ahead forecast, that predicts how much energy to buy from the grid to store it in the battery.

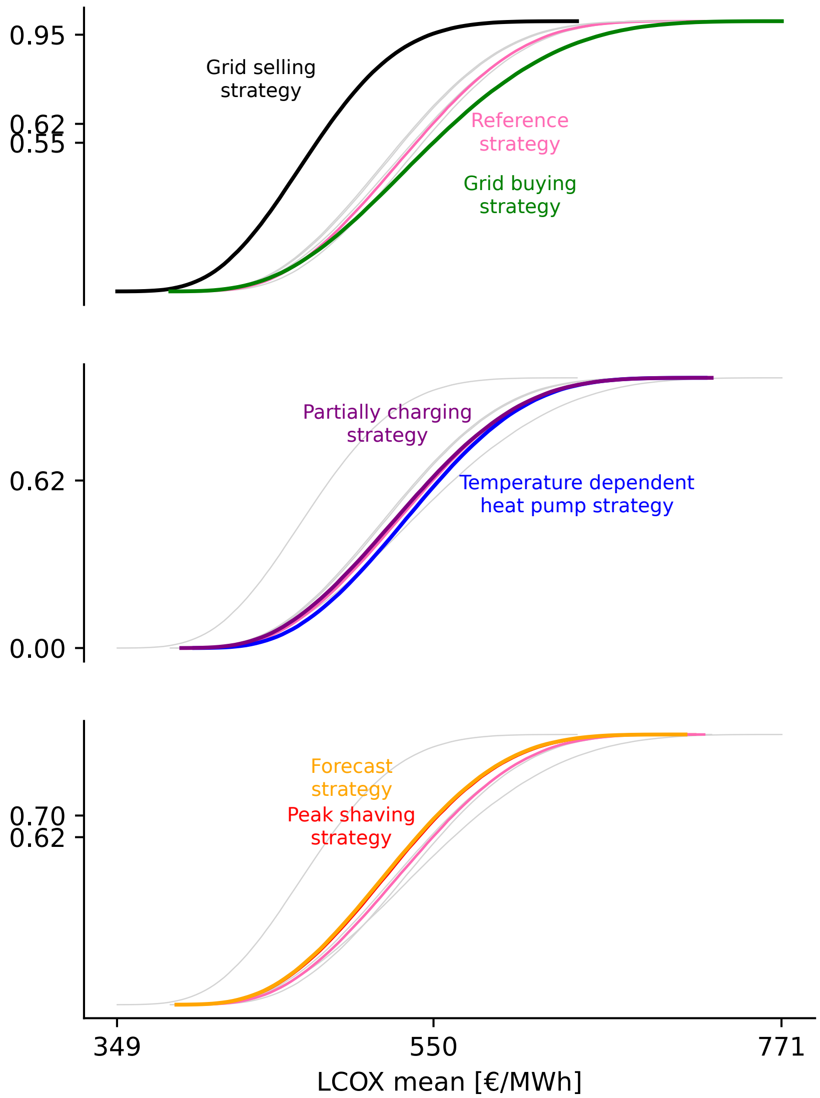

Figure 4.25: The Cumulative Density Function (CDF) of each strategy. The grid selling strategy, the forecast strategy and peak shaving strategy achieve a higher probability that the LCOX mean will be in reality below any predefined limit than the reference case.

Chapter 5

Conclusion

In this work, a robust design optimization has been done for a PV - battery - heat pump - thermal storage tank system for a household in Belgium. The system is subjected to various uncertainties (i.e. uncertainties on the loads, electricity cost and economic data). In the first part of the thesis, the model of the different components of the system has been explained. All elements are modeled in Python™. The NSGA-II algorithm is used to optimize the system and the polynomial chaos expansion method is used to propagate the different uncertainties. Each strategy has been evaluated in the multi-objective algorithm where both the LCOX standard deviation and LCOX mean are minimized. The results are a Pareto front with the optimal design variables characteristics and a sensitivity analysis of each uncertainty. Regarding the Pareto fronts of each strategy, a trade-off is observed between the objectives. Comparing each strategy with the reference scenario leads to different conclusions.

Firstly, the grid buying strategy achieves a higher LCOX standard deviation and mean up to 14% and 9% respectively than the reference case. Because it is directly buying electricity from the grid, it has higher grid costs and the system is more impacted by the grid electricity price and load uncertainties. This leads to weaker results regarding the LCOX. Looking at the grid selling strategy, it is shown that the optimizer tends to create as much PV power as possible. It is selling energy to the grid and stores almost no energy. All the designs have a

PV power of 10 kW_p and a battery capacity almost equal to 0kWh. Selling almost all its electricity surplus greatly benefited the system, leading to a smaller LCOX standard deviation and LCOX mean up to 20% and 13% respectively. Moreover, this strategy is the only one impacted by the uncertainty of the CAPEX of the PV. Reducing the uncertainty on the future investment costs of the PV further helps to improve the system's robustness. Consequently, the two strategies playing on the heat pump operation, the temperature dependent heat pump strategy and partially charging strategy, have similar results to the reference case. For the temperature dependent heat pump strategy, this can be explained by the threshold temperature equal to -3.9°C. Meaning that this strategy is following the reference scenario for more than 99% of the time. For the partially charging strategy, the part of the PV energy surplus going to the battery being always higher than 88%, the strategy is also mainly following the reference scenario. It can be concluded that even if the heat load is higher than the electricity load, due to the bad quality of heat, it is more interesting to first use the PV power surplus for the battery than the heat pump in an exergy environment. This result can be explained by the Carnot coefficient (see Equation 2.6). Finally, the two last presented strategies were the peak shaving strategy and forecast strategy. The Pareto front of the peak shaving strategy achieves better results than the reference case. This can be explained by the fact that it takes advantage of the peak and off-peak hours to optimally charge, discharge, buy or sell electricity. In the end, the system under this strategy can achieve a better LCOX mean and LCOX standard deviation (i.e. up to 1.2% and 1.8% respectively than the reference case). The last strategy, the forecast strategy, achieves a Pareto front showing improved results than the reference case. The system is able to optimally charge its battery for the coming hours at low costs. This strategy leads to the highest battery capacity to store the right amount of electricity. It can be concluded from these two strategies that have a more elaborated operation scheme, where it either takes advantage of the peak and off-peak hours or either has a day-ahead forecast, the system achieves better results and is less impacted by the uncertainties.

With the uncertainty quantification that has been performed, it is possible to see which uncertainties heavily impact the robustness of the different systems. It is shown that the two significant uncertainties are on the electricity price and on the electricity load. The electricity cost is the dominant one. Reducing the uncertainty around these parameters further helps to improve the standard deviation of the LCOX for all strategies. This means that once the future electricity mix is fixed, it is possible to have a more precise idea of the evolution of the electricity price. The electricity load depends on the prospective consumer behavior and loads (electric vehicle, connected objects, etc.). Subsequently, the uncertainties on the heat load and CAPEX of the ASHP also have an impact but lower than the two previous ones. This is mainly due to the reduced weight of heat in an exergy environment due to the Carnot coefficient, as mentioned earlier.

A final comparison between the strategies has been made based on the stochastic performance. A CDF for an optimal design has been constructed for the different strategies. It has been shown that if the household owner predefines an LCOX upper limit of 550€/MWh, the grid selling strategy achieves the highest probability (i.e. 95%) that the LCOX, in reality, will be below or equal to that upper limit. Comparing to the peak shaving strategy and forecast strategy, both give a probability of 70%. The temperature dependent heat pump, partially charging and heat pump strategies achieve a similar likelihood of 62%. The grid buying strategy has the worst probability of being below 550€/MWh (i.e. 55%).

As a final conclusion, this MSc thesis shows that it is possible to improve the system's performance by adopting an adequate power management strategy. Three characteristics can be found in these optimal strategies. Firstly, being able to sell electricity to the grid. Secondly, by having a different operation during peak and off-peak hours and thirdly, by making an optimal day-ahead loop to store energy at low costs. Subsequently, the uncertainty on the electricity price is dominant for the LCOX. Having a clear vision of the future energy mix of Belgium, further helps to improve the robustness of all the strategies.

Chapter 6

Future work

In this work, a PV - battery - heat pump - thermal storage tank for a household in Belgium has been optimized under different strategies and uncertainties. The model of this work can be further improved by dividing the heat load into hot sanitary water and space heating. Each type of heat demand requires a different hot water temperature. The final result will be different in an exergy environment. Subsequently, the heat pump model uses an approximation for the calculation of the COP. A more detailed approach could improve the results. Additional work can also be done by adding a hydrogen-based system to meet long-term storage requirements (seasonal). New strategies could be developed by taking advantage of this long-term storage. Moreover, the different strategies could be optimized for other techno-economic parameters such as efficiency, carbon emission, grid cost, etc. It could be interesting to see which design variables characteristics under a strategy can lead to the most negligible grid costs. Subsequently, as shown in the results, the electricity cost and electricity load have the most significant impact on the system performance. Reducing these uncertainties by studying the different future energy mixes or consumers' behavior could lead to new results. Finally, the strategies have been tested for a household located in Belgium, but evaluating them in another location with lower temperatures or higher solar irradiance could lead to different conclusions.

Acknowledgement

Computational resources have been provided by the supercomputing facilities of the Université catholique de Louvain (CISM/UCL) and the Consortium des Équipements de Calcul Intensif en Fédération Wallonie Bruxelles (CÉCI) funded by the Fond de la Recherche Scientifique de Belgique (F.R.S.-FNRS) under convention 2.5020.11 and by the Walloon Region.

Bibliography

[1] International Energy Agency. Renewables 2019: Analysis and forecast to 2024. *Tech. rep., International Energy Agency*, 2019.

[2] R. Luthander, J. Widén, D. Nilsson, and J. Palm. Photovoltaic self-consumption in buildings: A review. *Applied energy*, 142:80–94, 2015.

[3] H. Lund, P. A. Østergaard, D. Connolly, and B. V. Mathiesen. Smart energy and smart energy systems. *Energy*, 137:556–565, 2017.

[4] H. Lund, P. A. Østergaard, M. Chang, S. Werner, S. Svendsen, P. Sorknæs, J. E. Thorsen, F. Hvelplund, B. O. G. Mortensen, and B. V. Mathiesen et al. The status of 4th generation district heating: Research and results. *Energy*, 164:147–159, 2018.

[5] G. O. Gil, J. I. Chowdhury, N. Balta-Ozkan, Y. Hu, L. Varga, and P. Hart. Optimising renewable energy integration in new housing developments with low carbon technologies. *Renewable Energy*, 169:527–540, 2021.

[6] X. Wang, L. Xia, C. Bales, X. Zhang, B. Copertaro, S. Pan, and J. Wu. A systematic review of recent air source heat pump (ashp) systems assisted by solar thermal, photovoltaic and photovoltaic/thermal sources. *Renewable Energy*, 146:2472–2487, 2020.

[7] G. Mavromatidis, K. Orehounig, and J. Carmeliet. A review of uncertainty characterisation approaches for the optimal design of distributed energy systems. *Renewable and Sustainable Energy Reviews*, 88:258–277, 2018.

[8] N. Owen, P. Challenor, P. Menon, and S. Bennani. Comparison of surrogate- based uncertainty quantification methods for computationally expensive simulators. *SIAM/ASA Journal on Uncertainty Quantification*, 5:403–435, 2017.

[9] B. Sudret. Polynomial chaos expansions and stochastic finite element methods. *Risk and Reliability in Geotechnical Engineering (Chap. 6), K.-K. Phoon J. Ching (Eds.)*, pages 265–300, 2014.

[10] D. Coppitters, W. De Paepe, and F. Contino. Robust design optimization of a photovoltaic - battery - heat pump system with thermal storage under aleatory and epistemic uncertainty. *Energy*, 229, 2021.

[11] M. Liu, S. Wang, Y. Zhao, H. Tang, and J. Yan. Heat-power decoupling technologies for coal-fired chp plants: Operation flexibility and thermodynamic performance. *Energy*, 188, 2019.

[12] W. F. Holmgren, C. W. Hansen, and M. A. Mikofski. Pvlib python: a python package for modeling solar energy systems. *Journal of Open Source Software*, 3(29):884, 2018.

[13] W. De Soto et al. Improvement and validation of a model for photovoltaic array performance. *Solar Energy*, 80:78–88, 2006.

[14] G. de Oliveira e Silva and P. Hendrick. Lead–acid batteries coupled with pho- tovoltaics for increased electricity self-sufficiency in households. *Applied Energy*, 178:856–867, 2016.

[15] B. Battke, T. S. Schmidt, D. Grosspietsch, and V. H. Hoffmann. A review and probabilistic model of lifecycle costs of stationary batteries in multiple applications. *Renewable and Sustainable Energy Reviews*, 25:240– 250, 2013.

[16] S. Blaifi, S. Moulahoum, I. Colak, and W. Merrouche. An enhanced dynamic model of battery using genetic algorithm suitable for photovoltaic applications. *Applied Energy*, 169:888–898, 2016.

[17] B. Zakeri and S. Syrir. Electrical energy storage systems: A comparative life cycle cost analysis. *Renewable and sustainable energy reviews*, 42:569–596, 2015.

[18] B. Battke, T. S. Schmidt, D. Grosspietsch, and V. H. Hoffmann. A review and probabilistic model of lifecycle costs of stationary batteries in multiple applications. *Renewable and Sustainable Energy Reviews*, 25:240– 250, 2013.

[19] R. Dufo-Lopez, J. M. Lujano-Rojas, and J. L. Bernal-Agustín. Comparison of different lead–acid battery lifetime prediction models for use in simulation of stand-alone photovoltaic systems. *Applied Energy*, 115:242–253, 2014.

[20] C. Phurailatpam, B. S. Rajpurohit, and L. Wangın. Planning and optimization of autonomous dc microgrids for rural and urban applications in indias. *Renewable and Sustainable Energy Reviews*, 82:194–204, 2018.

[21] I. Pawel. The cost of storage - how to calculate the levelized cost of stored energy (lcoe) and applications to renewable energy generation. *Energy Procedia*, 46:68–77, 2014.

[22] P. Komor and J. Glassmire. Electricity storage and renewables for island power: a guide for decision makers. *International Renewable Energy Agency (IRENA)*.

[23] I. H. Bell, J. Wronski, S. Quoilin, and V. Lemort. Pure and pseudo-pure fluid thermophysical property evaluation and the open-source thermophysical property library coolprop. *Industrial Engineering Chemistry Research*, 53(6):2498–2508, 2014.

[24] G. Angenendt, S. Zurmuhlen, F. Rucker, H. Axelsen, and D. Uwe Sauer. Optimization and operation of integrated homes with photovoltaic battery t energy storage systems and power-to-heat coupling. *Energy Conversion and Management: X*, 1, 2019.

[25] R. W. Erickson. Dc–dc power converters. *Wiley Encyclopedia of Electrical and Electronics Engineering*, 2007.

[26] M. Taghvaee, M. Radzi, S. Moosavain, H. Hizam, and M. H. Marhaban. A current and future study on non-isolated dc–dc converters for photovoltaic applications. *Renewable and sustainable energy reviews*, 17:216–227, 2013.

[27] G. A. Rampinelli, A. Krenzinger, and F. Chenlo Romero. Mathematical models for efficiency of inverters used in grid connected photovoltaic systems. *Renewable and Sustainable Energy Reviews*, 34:578–587, 2014.

[28] S. Wilcox and W. Marion. Users manual for tmy3 data sets.

[29] Open energy information, commercial and residential hourly load profiles for all tmy3 locations in the united states.

[30] M. Montero Carrero, I. R. Sánchez, W. D. Paepe, A. Parente, and F. Contino. Is there a future for small-scale cogeneration in europe ? *Economic and Policy Analysis of the Internal Humid Air Turbine Cycles, Energies*, 12(3):1–27, 2019.

[31] R. Sangi, P. M. Martín, and D. Muller. Thermoeconomic analysis of a building heating system. *Energy*, 111:351–363, 2016.

[32] M. Di Somma, B. Yan, N. Bianco, G. Graditi, P. Luh, L. Mongibello, and V. Naso. Multi-objective design optimization of distributed energy systems through cost and exergy assessments. *Applied Energy*, 204:1299–1316, 2017.

[33] K. Verleysen. Unleash the power of hydrogen and other smart energy carriers. Master's thesis, Brussels Faculty of Engineering, Université Libre de Bruxelles, Vrije Universiteit Brussel, Brussels, 2018.

[34] M. Mitchell. Genetic algorithms: An overview1. *Complexity*, 1(1):31–39, 1995.

[35] A. Konak, D. W. Coit, , and A. E. Smith. Multi-objective optimization using genetic algorithms: A tutorial. *Reliability Engineering System Safety*, 91(9):992– 1007, 2006.

[36] M. Stein. Large sample properties of simulations using latin hypercube sampling. *Technometrics*, 29(2):143–151, 1987.

[37] A. Olivier, D.G. Giovanis, B.S. Aakash, M. Chauhan, L. Vandanapu, and M.D. Shields. Uqpy: A general purpose python package and development environment for uncertainty quantification. *Journal of Computational Science*, 2020.

[38] P. Tsirikoglou, S. Abraham, F. Contino, Ö. Bağcı, J. Vierendeels, and G. Ghorbaniasl. Comparison of metaheuristics algorithms on robust design optimization of a plain-fin-tube heat exchanger. 18th AIAA/ISSMO Multidisciplinary Analysis and Optimization Conference, 2017.

[39] S. Gendebien, E. Georges, S. Bertagnolio, and V. Lemort. Methodology to characterize a residential building stock using a bottom-up approach: a case study applied to belgium. *International Journal of Sustainable Energy Planning and Management*, 4:71–88, 2014.

[40] Climact. *Electrical energy savings scenarios for Belgium, Tech. rep., Climact*, 2012.

[41] W. Tian, Y. Heo, P. De Wilde, Z. Li, D. Yan, C. S. Park, X. Feng, and G. Augenbroe. A review of uncertainty analysis in building energy assessment. *Renewable and Sustainable Energy Reviews*, 93:285–301, 2018.

[42] Elia. Electricity scenarios for belgium towards 2050: Elia's quantified study on the energy transition in 2030 and 2040. *Tech. rep., Elia*, 2017.

[43] PricewaterhouseCoopers. Vergelijking van de elektriciteitsen aardgastarieven, tech. rep., vlaamse regulator van de elektriciteits- en gasmarkt. 2019.

[44] N. Lukač, S. Seme, K. Dezan, B. Zalik, and G. Stumberger. Economic and environmental assessment of rooftops regarding suitability for photovoltaic systems installation based on remote sensing data. *Energy*, 107:854– 865, 2016.

[45] K. K. Cao, A. N. Nitto, E. Sperber, and A. Thess. Expanding the horizons of power-to-heat: Cost assessment for new space heating concepts with wind powered thermal energy systems. *Energy*, 164:925–936, 2018.

[46] Vaillant allstor exclusiv. `https://www.vaillant.be/consumenten/producten/allstor-exclusiv-2048.html`. Accessed: 22.10.2020.

[47] Eco-star allstor exclusiv. `https://www.va-shop.be`. Accessed: 22.10.2020.

[48] T. H. T. Nguyen, T. Nakayama, and M. Ishida. Optimal capacity design of battery and hydrogen system for the dc grid with photovoltaic power generation based on the rapid estimation of grid dependency. *International Journal of Electrical Power Energy Systems*, 89:27–39, 2017.

[49] A. Khiareddine, C. B. Salah, D. Rekioua, and M. F. Mimouni. Sizing methodology for hybrid photovoltaic/wind/hydrogen/battery integrated to energy management strategy for pumping system. *Energy*, 153:743–762, 2018.

[50] A. Singh, P. Baredar, and B. Gupta. Techno-economic feasibility analysis of hydrogen fuel cell and solar photovoltaic hybrid renewable energy system for academic research building. *Energy Conversion and Management*, 145:398–414, 2017.

[51] G. Blatman and B. Sudret. Adaptive sparse polynomial chaos expansion based on least angle regression. *J. Comput. Phys.*, 230:2345–2367, 2011.

[52] H. Najm. Uncertainty quantification and polynomial chaos techniques in computational fluid dynamics. *Annu. Rev. Fluid Mech.*, 41(1):35–52, 2009.

[53] S. Abraham et al. A robust and efficient stepwise regression method for building sparse polynomial chaos expansions. *J. Comput. Phys.*, 2016.

[54] S. Hosder, R. Walters, and M. Balch. Efficient sampling for non-intrusive polynomial chaos applications with multiple uncertain input variables, in: Aiaa 2007-1939, 48th aiaa/asme/asce/ahs/asc structures. Structural Dynamics and Material Conference, Honolulu, Hawaii, 2007.

[55] X. Wei, H. Chang, B. Fend, and Z. Liu. Sensitivity analysis based on polynomial chaos expansions and its application in ship uncertainty-based design optimization. *Mathematical Problems in Engineering*, 2019.

[56] G. Xianguang, S. Guangyong, L. Guangyao, M. Lichen, and L. Qing. A comparative study on multiobjective reliable and robust optimization for crashworthiness design of vehicle structure. *Structural and Multidisciplinary Optimization*, 48:669–684, 2014.

UNIVERSITÉ CATHOLIQUE DE LOUVAIN
École polytechnique de Louvain
Rue Archimède, 1 bte L6.11.01, 1348 Louvain-la-Neuve, Belgique | **www.uclouvain.be/epl**